arXiv:2112.00037v3 [astro-ph.CO] 13 Jun 2022

Pseudoscalar sterile neutrino self-interactions in light of Planck, SPT and ACT data

Mattia Atzori Corona,[a,b] **Riccardo Murgia,**[c,h] **Matteo Cadeddu,**[b] **Maria Archidiacono,**[d,e] **Stefano Gariazzo,**[f] **Carlo Giunti,**[f] **Steen Hannestad**[g]

[a]Dipartimento di Fisica, Università degli Studi di Cagliari, Complesso Universitario di Monserrato - S.P. per Sestu Km 0.700, 09042 Monserrato, Italy

[b]INFN – Istituto Nazionale di Fisica Nucleare, Sezione di Cagliari, Complesso Universitario di Monserrato - S.P. per Sestu Km 0.700, 09042 Monserrato, Italy

[c]LUPM – Laboratoire Univers & Particules de Montpellier, CNRS & Université de Montpellier (UMR-5299), Place Eugène Bataillon, F-34095 Montpellier Cedex 05, France

[d]Università degli Studi di Milano, via G. Celoria 16, 20133 Milano, Italy

[e]INFN – Istituto Nazionale di Fisica Nucleare, Sezione di Milano, Via G. Celoria 16, 20133 Milano, Italy

[f]INFN – Istituto Nazionale di Fisica Nucleare, Sezione di Torino, Via P. Giuria 1, 10125 Turin, Italy

[g]Department of Physics and Astronomy, Aarhus University, DK-8000 Aarhus C, Denmark

[h]Gran Sasso Science Institute (GSSI), I-67100 L'Aquila, Italy

E-mail: mattia.atzori.corona@ca.infn.it, riccardo.murgia@gssi.it, matteo.cadeddu@ca.infn.it, maria.archidiacono@unimi.it, gariazzo@to.infn.it, carlo.giunti@to.infn.it, steen@phys.au.dk

Abstract. We reassess the viability of a cosmological model including a fourth additional sterile neutrino species that self-interacts through a new pseudoscalar degree of freedom. We perform a series of extensive analyses fitting various combinations of cosmic microwave background (CMB) data from *Planck*, the Atacama Cosmology Telescope (ACT) and the South Pole Telescope (SPT), both alone and in combination with Baryon Acoustic Oscillation (BAO) and Supernova Ia (SnIa) observations. We show that the scenario under study, although capable to resolve the Hubble tension without worsening the so-called S_8 tension about the growth of cosmic structures, is severely constrained by high-multipole polarization data from both *Planck* and SPT. Intriguingly, when trading *Planck* TE-EE data for those from ACT, we find a $\gtrsim 3\sigma$ preference for a non-zero sterile neutrino mass, $m_s = 3.6^{+1.1}_{-0.6}$ eV (68% C.L.), compatible with the range suggested by longstanding short-baseline (SBL) anomalies in neutrino oscillation experiments. The pseudoscalar model provides indeed a better fit to ACT data compared to ΛCDM ($\Delta\chi^2 \simeq -5$, ΔAIC $= -1.3$), although in a combined analysis with *Planck* the ΛCDM model is still favoured, as the preference for a non-zero sterile neutrino mass is mostly driven by ACT favouring a higher value for the primordial spectral index n_s with respect to *Planck*. We show that the mild tension between *Planck* and ACT is due to the different pattern in the TE and EE power spectra on multipoles between $350 \lesssim \ell \lesssim 1000$. We also check the impact of marginalizing over the gravitational lensing information in *Planck* data, showing that the model does not solve the CMB lensing anomaly. Future work including higher precision data from current and upcoming CMB ground-based experiments will be crucial to test these results.

Contents

1 Introduction

The Λ Cold Dark Matter (ΛCDM) cosmological model has been proven to provide an excellent fit both to early-universe observations, such as the cosmic microwave background (CMB) [1], and to late-universe measurements, such as large-scale structure data (LSS) data [2, 3]. Nonetheless, within such a standard framework there exist a few tensions, most notably between the early-universe, indirect determinations of the Hubble parameter H_0 and of the parameter $S_8 \equiv \sigma_8(\Omega_m/0.3)^{0.5}$ – where σ_8 is the root mean square of matter fluctuations on a 8 h^{-1}Mpc scale, and Ω_m is the total matter abundance – compared to their direct, low-redshift measurements, respectively from calibrated SnIa as a cosmic distance ladder [4–12] and weak gravitational lensing [13–18]. In spite of meticulous attempts to check for possibly unaccounted systematics at play in the local estimates of such parameters [17, 19, 20], both the so-called Hubble and growth tensions persist, and have nowadays reached about the 5 and 3 σ level, respectively [21–25].

While a resolution to the growth tension can be achieved in a number of models departing from ΛCDM at late times without affecting pre-recombination physics (e.g. [26–30]), purely late-time explanations of the Hubble tension have been shown to be the least viable,

due to the SnIa and BAO constraints at $z \lesssim 2$ [31, 32]. However, currently there is an open debate on the possibility that introducing new physics in the pre-recombination era could resolve the Hubble tension without spoiling other bounds or exacerbating the growth tension [21, 32–35]. It seems indeed that, in order to fully restore cosmological concordance, it might be necessary to modify both the early-universe physics, e.g. by reducing the sound horizon at recombination to accommodate a higher H_0, and the late-universe physics, to decrease the amplitude of matter fluctuations on scales $k \sim 0.1 - 1 \ h/\mathrm{Mpc}$ [34, 36]. One possibility, motivated by particle physics [37, 38] is the introduction of a light sterile neutrino species, namely a singlet state under the $\mathrm{SU}(2)_L \otimes \mathrm{U}(1)_Y$ electroweak gauge group. This additional degree of freedom would not interact via any of the fundamental interactions of the Standard Model, but would oscillate with the active neutrino species.

The existence of a sterile neutrino with a mass in the eV range is motivated by the fact that it might provide an explanation to long-standing anomalies in short-baseline (SBL) neutrino oscillation experiments. These include the anomalous appearance of events measured by the LSND [39] and MiniBooNE [40, 41] experiments, and the anomalous disappearance of electron (anti)neutrinos detected by several observations measuring the electron antineutrino flux from nuclear reactors [42] and in the calibration of the GALLEX [43] and SAGE [44] gallium solar neutrino experiments [45, 46] (see Refs. [38, 47, 48] for a full list of references). Although the sterile neutrino hypothesis was claimed to provide an explanation to all these anomalies at once [47, 49], the tension between appearance and disappearance channels has increased to a very strong level in the recent years [50–52]. Moreover, recent re-analyses of the reactor data [53, 54] have reduced the significance of the reactor antineutrino anomaly. On the other hand, the Gallium anomaly, which was reduced by the shell model reevaluation of the cross section in Ref. [55], has been recently revived by the result of the BEST experiment [56] (see also the discussions in Refs. [54, 57, 58]). Considering the $\nu_\mu \to \nu_e$ appearance channel, the new results of the MicroBooNE experiment [59–61] disfavour the sterile neutrino interpretation of the MiniBooNE anomaly as an electron neutrino appearance from a muon neutrino beam (see, however, the discussion in Ref. [62]). It is interesting that a recent analysis shows a 2.2σ preference for a sterile neutrino mass in the eV scale if the MicroBooNE data are interpreted in terms of electron neutrino disappearance [63].

CMB and LSS observations strongly constrain the simplest scenario where the new sterile neutrino component is a non-interacting and free-streaming species [47, 64–67]. In such a minimal scenario, it is therefore very unlikely to find a common resolution to SBL anomalies and cosmological tensions. That is why several models beyond the simple non-interacting case have been proposed in the literature, in particular scenarios where the sterile neutrinos are coupled through new interactions [68–71].

In this work, we focus on a specific self-interacting sterile neutrino scenario – introduced in Refs. [70, 72] and subsequently tested against cosmological and SBL data in Refs. [73, 74] – where a light massive sterile neutrino species self-interacts through the exchange of a new massless pseudoscalar degree of freedom. This model induces a radically different phenomenology compared to the non-interacting case, because the sterile neutrino is not a free-streaming species. In fact, due to its self-interaction, it can be treated as a single tightly coupled fluid together with the pseudoscalar. Moreover, the rapid pair-annihilation and disappearance when the temperature drops below its mass prevents the pseudoscalar model from violating constraints from LSS observations [70, 72]. Although this scenario can readily ease the Hubble tension, a non-zero sterile neutrino mass, mildly favoured by *Planck* CMB temperature data [73], appears to be very tightly constrained when high-multipole *Planck*

polarization data are added to the analysis [74].

Let us now introduce another anomaly characterizing the standard cosmological framework: the so-called CMB lensing (or "$A_{\rm lens}$") anomaly, i.e. a residual oscillatory feature in *Planck* data at high multipoles ($1000 \lesssim \ell \lesssim 2000$) compared to the best-fit ΛCDM prediction [1, 75–77]. Such a feature can be described as an extra source of smoothing of the acoustic peaks, and modelled via two extra phenomenological parameters: $A_{\rm L}^{\rm TTTEEE}$, that controls the amount of smoothing, and $A_{\rm L}^{\phi\phi}$, that re-scales the global amplitude of the lensing potential power spectrum. Both these parameters are predicted to be equal to one within the ΛCDM model. While the lensing anomaly can be observed in the TT-TE-EE spectra, the amount of gravitational lensing can also be determined directly from the lensing potential power spectrum reconstructed from the CMB four-point correlation function, and in this case it is compatible with the ΛCDM expectation ($A_{\rm L}^{\phi\phi} = 1$). On the other hand, the case where $A_{\rm L}^{\rm TTTEEE} = 1$ is about 3σ away from the ΛCDM best-fit. It thus seems that the extra smoothing of the TT-TE-EE peaks cannot be attributed to actual gravitational lensing [76, 78, 79]. Furthermore, once marginalizing over the lensing information in *Planck* data, the resulting temperature and polarization power spectra favor a cosmology with a lower A_s and $\omega_{\rm cdm} \equiv \Omega_{\rm cdm} h^2$. Indeed, these parameters are strongly correlated with the amplitude of the lensing potential power spectrum. As a consequence, the "ΛCDM+$A_{\rm lens}$" cosmology shows no growth tension and a slightly alleviated Hubble tension. Moreover, such a cosmology is in better agreement with the ΛCDM best-fit cosmology reconstructed from data collected by ongoing ground-based CMB experiments at the South Pole Telescope (SPT) [80, 81] and Atacama Cosmology Telescope (ACT) [82, 83] (see, e.g. Ref. [84]). No departure from the case where $A_{\rm L}^{\rm TTTEEE} = 1$ is indeed preferred by SPT and ACT. The introduction of $A_{\rm L}^{\rm TTTEEE}$ and $A_{\rm L}^{\phi\phi}$ modify the correlation between cosmological parameters both in the presence of an additional free-streaming component, as in the non-interacting sterile neutrino model, and in the pseudoscalar scenario, where the sterile neutrino component behaves like a coupled fluid rather than a free-streaming species. It is thus worth studying whether such a multi-parameter degeneracy can alleviate the lensing anomaly in each of these two scenarios, as well as investigating the impact on the sterile neutrino sector parameters.

In light of all these considerations, our goal is to test the robustness of the limits obtained in Ref. [74] under the following changes in the CMB data analysis:

- trading the high-multipole TE-EE data from *Planck* for those from SPT[1], as in Refs. [81, 86, 87];

- trading the high-multipole TE-EE data from *Planck* for those from ACT, as in Refs. [87–91].

- introducing two additional free parameters, $A_{\rm L}^{\rm TTTEEE}$ and $A_{\rm L}^{\phi\phi}$, the former capturing the impact of gravitational lensing on the TT-TE-EE spectra, the latter globally re-scaling the amplitude of the lensing potential power spectrum, in order to marginalize over the lensing anomaly in *Planck* data, as in Refs. [87, 92–94];

---

[1]We made use of the SPTpol data and likelihood, being the only publicly available likelihood for SPT data that can be interfaced with the MCMC sampler used in this work. A more recent data-set, SPT-3G [85], was released by the SPT Collaboration when our work was already in an advanced stage. We leave an analysis of the pseudoscalar scenario with SPT-3G data for a future work.

This work is structured as follows: in Sec. 2 we briefly outline the theoretical framework under study; in Sec. 3 we discuss the data-sets that we have considered and the methodology that we have adopted; in Sec. 4 we present our results; Sec. 5 is dedicated to a deeper scrutiny of the analyses with ACT data; in Sec. 6 we briefly discuss the compatibility of our cosmological results with up-to-date constraints from SBL neutrino oscillation experiments; finally, in Sec. 7 we draw our conclusions and outline future perspectives.

2   The pseudoscalar sterile neutrino self-interaction model

The theoretical framework under investigation – introduced in Ref. [70] and subsequently reassessed in light of different experimental constraints in Refs. [70, 72–74] – is a cosmological scenario where a sterile neutrino species couples to an effectively massless pseudoscalar degree of freedom. In this Section we briefly recall its basic features and phenomenological parametrisation.

The Lagrangian term describing the coupling between sterile neutrinos and the new pseudoscalar field ϕ, with mass $m_\phi \ll 1$ eV, is given by:

$$\mathcal{L} \sim g_s \phi \bar{\nu}_4 \gamma^5 \nu_4, \tag{2.1}$$

where ν_4 is the fourth – mainly sterile – neutrino mass state, and g_s is the coupling constant that characterizes the intensity of the interaction. The new interaction is also partly felt by active neutrinos, although in this case its strength is suppressed by the active-sterile mixing angle. If the dimensionless coupling is larger than $g_s \sim 10^{-6}$, the production of sterile neutrinos, which causes an increase of $N_{\rm eff}$, is delayed until the time of active neutrino decoupling when active-sterile oscillations are not effective anymore. This moment also roughly coincides with the onset of BBN, allowing to evade the bounds from the latter [95]. After neutrinos decouple from the plasma, the energy in the neutrino-pseudoscalar sector is redistributed by oscillations so that the sterile plus pseudoscalar sector ends up with a fraction of $11/32$ of the total energy density, while the remaining fraction $21/32$ goes to the active sector. After that, provided that $g_s \gtrsim 10^{-6}$, the active neutrinos and the sterile-pseudoscalar components are completely decoupled and do not exchange neither energy nor momentum. The sterile neutrinos become very strongly coupled with the pseudoscalar field and the system can be treated as a single fluid with a well-defined energy density and equation of state. As soon as sterile neutrinos become non-relativistic, they annihilate into ϕ, which is effectively massless, so that this mechanism allows evading limits on the neutrino mass arising from LSS. For these reasons, whereas the non-interacting sterile neutrino parameter space is strongly constrained by the aforementioned cosmological probes, the pseudoscalar model could potentially allow to reconcile O(eV) sterile neutrinos with cosmology. Given that the value of g_s has an unique correspondence with the effective number of relativistic degrees of freedom $N_{\rm eff}$ (see Fig.1 from Ref. [70]), the pseudoscalar model features only two additional free parameters: the sterile neutrino mass m_s, and its contribution to the effective number of relativistic degrees of freedom $\Delta N_{\rm eff}$. We address the reader to the aforementioned Refs. [70, 72–74] for a comprehensive description of the model.

3   Methods and data

We test the pseudoscalar self-interacting sterile neutrino model on a number of cosmological observations, by means of a set of comprehensive Markov Chain Monte Carlo (MCMC)

analyses with the `MontePython-v3`[2] sampler [96, 97], interfaced with a modified version of the numerical Einstein-Boltzmann solver `CLASS` [74, 98]. We consider various combinations of the following data-sets:

- the low-ℓ CMB TT, EE ($\ell < 30$), the high-ℓ TT, TE, EE ($30 \leq \ell \leq 2500$) data [1], and the gravitational lensing potential reconstruction ($8 \leq \ell \leq 400$) [99] from *Planck* 2018;

- the high-ℓ CMB EE and TE ($50 \leq \ell \leq 8000$) [80] measurements, and the reconstructed gravitational lensing potential ($100 \leq \ell \leq 8000$) [100] from the 500deg SPTpol survey [81];

- the high-ℓ CMB TT, EE and TE ($350 \leq \ell \leq 4125$) data from the DR4 of the ACT survey [82, 83];

- the BAO measurements from 6dFGS at $z = 0.106$ [101], SDSS DR7 at $z = 0.15$ [102], BOSS DR12 at $z = 0.38, 0.51$ and 0.61 [2], and the joint constraints from eBOSS DR14 Ly-α auto-correlation at $z = 2.34$ [103] and cross-correlation at $z = 2.35$ [104];

- the measurements of the growth function $f\sigma_8(z)$ (FS) from the CMASS and LOWZ galaxy samples of BOSS DR12 at $z = 0.38, 0.51$, and 0.61 [2];

- the Pantheon SnIa catalogue, spanning redshifts $0.01 < z < 2.3$ [105].

Our baseline cosmology is described by the standard set of six ΛCDM parameters, namely the baryon and cold dark matter physical energy densities (ω_b, $\omega_{\rm cdm}$), the angular size of the sound horizon at recombination (θ_s), the tilt and amplitude of the primordial power spectrum (n_s, A_s), and the optical depth at reionization ($\tau_{\rm reio}$). The pseudoscalar scenario is fully characterized by two additional parameters describing the sterile neutrino sector, i.e. the sterile neutrino mass, m_s, and its contribution to the effective number of relativistic degrees of freedom, $\Delta N_{\rm eff}$. We adopt flat priors on all the parameters[3], and we assume massless active neutrinos for simplicity. We consider MCMC chains to be converged when the Gelman-Rubin criterion [106] satisfies $R - 1 < 0.03$. We analyze the results with the `Getdist` python package[4] [107], and extract best-fit parameters making use of the Minuit algorithm [108] through the `iMinuit` python package[5]. We primarily focus on the results in each of the CMB-only set-ups that we have considered, and then discuss the impact of adding BAO and SnIa data to the analyses.

4 Results

Let us first briefly discuss the current constraints on the pseudoscalar model from *Planck* data, that are shown as empty black contours in Fig. 1, together with the limits from the other data combinations that will be discussed in the following Subsections. As a reference, we also report *Planck* limits on the ΛCDM model and the bands representing the direct measurement

---

[2]https://github.com/brinckmann/montepython_public

[3]When making use of ACT data, we adopt a Gaussian prior on the optical depth to reionization, $\tau_{\rm reio} = 0.06 \pm 0.01$, as suggested by the ACT collaboration, to overcome the lack of information on low multipoles. We verified that including low-ℓ EE data from *Planck* rather than adopting such a prior choice on $\tau_{\rm reio}$ does not affect our conclusions.

[4]https://getdist.readthedocs.io/
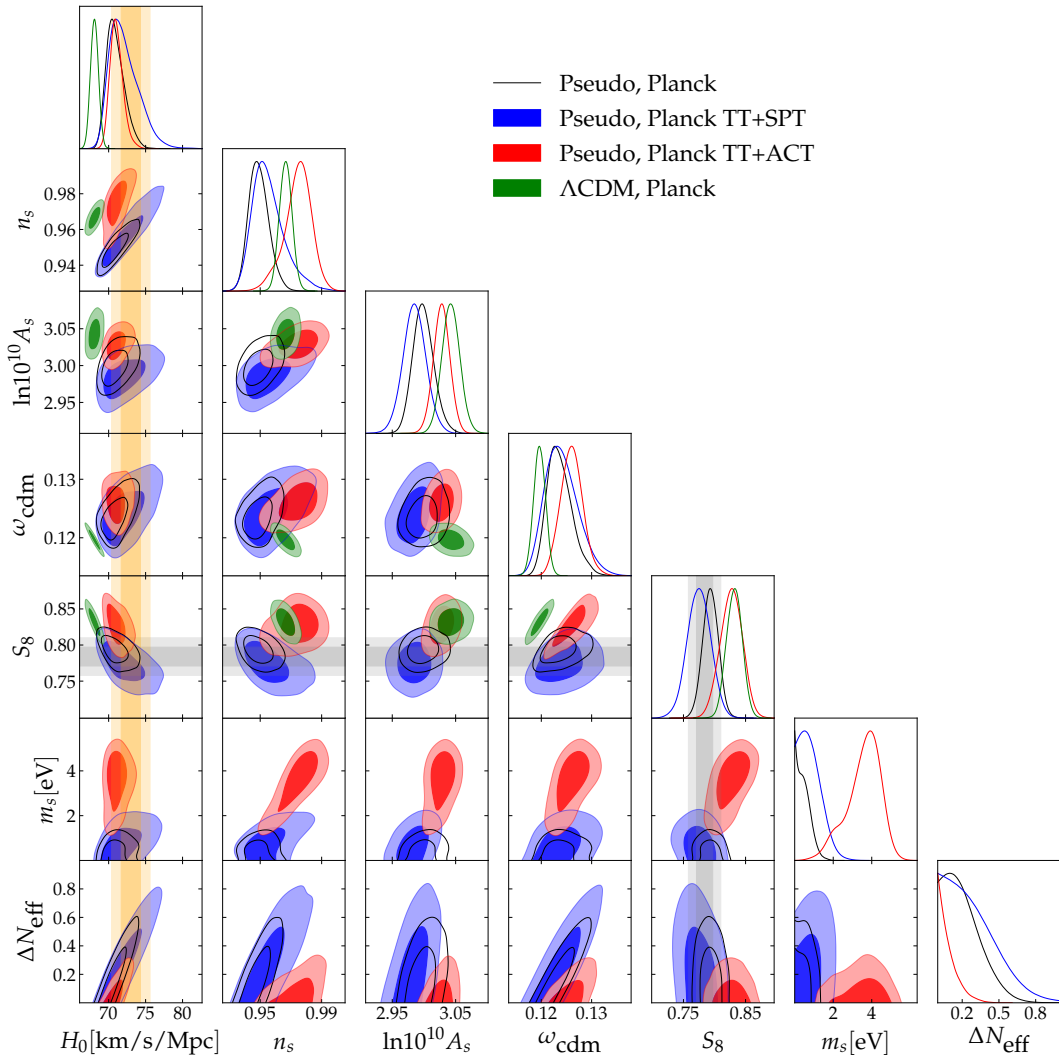
[5]https://iminuit.readthedocs.io/

Figure 1. Posterior distributions of the cosmological parameters in the ΛCDM and pseudoscalar (Pseudo) model for different CMB data-sets. The orange and gray bands represent the direct measurements (1σ and 2σ confidence regions) of H_0 and S_8, from cosmic distance ladder [9] and weak lensing observations [18], respectively.

of the Hubble constant from cosmic distance ladder ($H_0 = 73.0^{+1.3}_{-1.3}$ km/s/Mpc [9]) and S_8 from weak lensing observations ($S_8 = 0.784^{+0.013}_{-0.013}$ [18]). The corresponding mean values and $\pm 1\sigma$ C.L. are reported in the first column of Tab. 1. We substantially confirm the capability of the model under study to provide higher values for H_0 with respect to ΛCDM, mostly because of the well-known degeneracy between the latter parameter and the extra-contribution to the effective number of relativistic degrees of freedom $\Delta N_{\rm eff}$. It is also interesting to notice that the pseudoscalar scenario predicts lower values for the amplitude and tilt of the primordial power spectrum, A_s and n_s, resulting in a lower value for S_8, so that the model could in principle resolve both the Hubble tension and the growth tension. However, as already extensively discussed in Ref. [74], *Planck* polarization data on multipoles larger than $\ell = 30$ severely constrain the possibility of a non-zero sterile neutrino mass. The degradation of the

	Pseudo vs CMB			
Parameter	*Planck*	*Planck* w. $A_{\rm lens}$	*Planck* TT+SPT	*Planck* TT+ACT
$100\,\omega_b$	$2.269^{+0.025}_{-0.025}$	$2.319^{+0.030}_{-0.032}$	$2.272^{+0.032}_{-0.036}$	$2.216^{+0.018}_{-0.022}$
$\omega_{\rm cdm}$	$0.1237^{+0.0020}_{-0.0029}$	$0.1223^{+0.0027}_{-0.0035}$	$0.1239^{+0.0026}_{-0.0038}$	$0.1261^{+0.0022}_{-0.0023}$
$100\,\theta_s$	$1.04530^{+0.00040}_{-0.00043}$	$1.04530^{+0.00043}_{-0.00046}$	$1.04510^{+0.00049}_{-0.00054}$	$1.04670^{+0.00049}_{-0.00042}$
$\ln 10^{10}A_s$	$2.999^{+0.015}_{-0.018}$	$2.974^{+0.020}_{-0.018}$	$2.985^{+0.018}_{-0.018}$	$3.028^{+0.013}_{-0.013}$
n_s	$0.9491^{+0.0057}_{-0.0073}$	$0.9634^{+0.0079}_{-0.0096}$	$0.955^{+0.007}_{-0.013}$	$0.975^{+0.010}_{-0.007}$
$\tau_{\rm reio}$	$0.0589^{+0.0073}_{-0.0087}$	$0.0506^{+0.0089}_{-0.0079}$	$0.0522^{+0.0082}_{-0.0078}$	$0.0550^{+0.0060}_{-0.0062}$
m_s [eV]	< 1.1	< 1.0	< 1.9	$3.6^{+1.1}_{-0.6}$
$\Delta N_{\rm eff}$	< 0.50	$0.37^{+0.17}_{-0.25}$	< 0.67	< 0.25
$A_{\rm L}^{\phi\phi}$		$1.132^{+0.044}_{-0.048}$		
$A_{\rm L}^{\rm TTTEEE}$		$1.241^{+0.073}_{-0.080}$		
H_0 [km/s/Mpc]	$71.0^{+1.0}_{-1.5}$	$73.8^{+1.6}_{-2.1}$	$72.1^{+1.4}_{-2.4}$	$71.1^{+0.8}_{-1.0}$
S_8	$0.794^{+0.013}_{-0.013}$	$0.744^{+0.019}_{-0.019}$	$0.775^{+0.018}_{-0.020}$	$0.828^{+0.019}_{-0.018}$

Table 1. The mean $\pm 1\,\sigma$ error ($2\,\sigma$ in the case of upper bounds) of the cosmological parameters from CMB experiments in the pseudoscalar model.

global fit with respect to ΛCDM ($\Delta\chi^2 \simeq 13$) is indeed fully driven by a poor fit to that subset of *Planck* data (see App. A, where we report all individual χ^2's).

4.1 Planck TT+SPT

Let us now shortly discuss the constraints on the pseudoscalar model obtained from a set of CMB data constituted by low-ℓ temperature and polarization as well as high-ℓ temperature data from *Planck*, in combination with high-ℓ polarization data from SPT. The resulting contour plots are shown in blue in Fig. 1, while the corresponding mean values and $\pm 1\sigma$ C.L. are reported in the third column of Tab. 1. From Fig. 1 we clearly see that the *Planck* TT+SPT contours are very similar to the *Planck*-only ones, albeit with larger uncertainties. As in the ΛCDM case [80, 81], even in the pseudoscalar model the inclusion of SPT data favours low S_8 values in agreement with weak lensing observations. However, we find a degradation of the fit with respect to ΛCDM, which is mainly driven by a worse fit to *Planck* high-ℓ TT data ($\Delta\chi^2 \simeq 8$), and by a mild degradation in the fit to TE and EE data from SPT ($\Delta\chi^2 \simeq 3$).

From this analysis we conclude that the SPT data-set used in this work does not provide enough constraining power to significantly impact *Planck* results. For this reason, very similar conclusions could be drawn from our *Planck* and *Planck* TT+SPT analyses. Let us stress that, given the large uncertainties of SPT data, the tight limits on the sterile neutrino sector obtained within this data-combination are strongly driven by *Planck*. As one can see by comparing the black and blue contours of Fig. 1, the addition of SPT data actually relaxes the bounds, allowing a larger overlap with the predictions from *Planck* TT+ACT, that we will extensively discuss in the following Sections. Hence, it will be extremely important to confront the pseudoscalar model with the latest, higher-precision data release from SPT-3G [85]. We leave such a study for a future work.

4.2 Planck TT+ACT

We now discuss the results obtained performing a joint analysis of *Planck* low-ℓ + high-ℓ TT data, combined with the ACT DR4 data-set[6], that are reported in red in Fig. 1. The corresponding mean values and $\pm 1\sigma$ C.L. are listed in the last column of Tab. 1. As it is

---

[6]We follow the procedure suggested by the ACT collaboration and truncate multipoles $\ell < 1800$ in the ACT TT data to prevent double counting of modes.

manifest from both Fig. 1 and Tab. 1, the inclusion of ACT data drives n_s towards higher values, both in the ΛCDM and in the pseudoscalar model. However, in the ΛCDM scenario the predictions from the three different data-sets shown in Fig. 1 are consistent within 1σ. On the other hand, driven by the fact that ACT data favour $n_s \sim 1$ – although with large error bars – in the pseudoscalar scenario the result from *Planck* TT+ACT ($n_s = 0.975^{+0.010}_{-0.007}$) is roughly 2σ larger than what we find in the *Planck* and *Planck* TT+SPT analyses, i.e. $n_s = 0.9491^{+0.0057}_{-0.0073}$ and $0.955^{+0.007}_{-0.013}$, respectively. Strikingly, in the *Planck* TT+ACT analysis the positive correlation between n_s and m_s, as apparent in Fig. 1, leads to a preference for a non-zero sterile neutrino mass of $m_s = 3.6^{+1.1}_{-0.6}$ eV (68% C.L.). In other words, within ΛCDM, given the absence of an extra-parameter capable to balance the effect of a higher n_s, the difference between *Planck* and ACT predictions translates into a lower n_s – though still slightly higher than that favoured by *Planck* alone – and thus a degradation of the fit to ACT data. Conversely, in the pseudoscalar scenario the goodness of the fit to ACT data is not altered by the addition of *Planck* TT data, there is more room for a relatively high n_s, and consequently higher values of m_s are allowed. We will discuss more in detail the degeneracy between the tilt of the primordial power spectrum and the sterile neutrino mass in Sec. 5, where we carry out a more extensive investigation on the constraints reported here, aimed at identifying the range of multipoles where ACT and *Planck* and polarization data are somewhat in tension.

The preference for a larger value of n_s (and A_s) also translates into higher values for S_8, that consequently would be at odds roughly as much as the ΛCDM prediction with what is measured by weak lensing surveys. The parameter $\Delta N_{\rm eff}$ is severely constrained, as one can also see from the last column of Tab. 1. Let us finally note that in the joint *Planck* TT+ACT data-set the global fit is only mildly degraded compared to ΛCDM ($\Delta\chi^2 \simeq 3$), due to the fact that the pseudoscalar model provides a better fit of ACT data than the ΛCDM model ($\Delta\chi^2 \simeq -6$), balancing the worse fit to high-ℓ *Planck* TT data ($\Delta\chi^2 \simeq 9$).

4.3 Best-fit cosmologies and impact on the CMB power spectra

Let us now explicitly compare the different best-fit CMB angular power spectra from the various analyses that we just discussed. In Fig. 2 we show the residuals in the CMB TT, EE and TE power spectra for the pseudoscalar model tested against *Planck*, *Planck* TT+SPT, *Planck* TT+ACT data together with *Planck* and ACT data-points and error bars. For comparison, we also show the residuals of the ΛCDM tested against *Planck* TT+ACT.

In all cases the residuals are computed with respect to the ΛCDM best-fit from *Planck*-only. From Fig. 2, as expected, we first note that the best-fit spectra from the Planck TT+SPT analysis are very similar to those from the *Planck*-only analysis. Most importantly, we notice that the *Planck* TT+ACT case, being the only data combination favouring a non-zero value of m_s, features indeed the most significant differences in the angular power spectra, especially in TE and EE. Notice also that the enhanced oscillation pattern around $\ell \sim 500$ resembles the best-fit power spectrum obtained in the *Planck* TT only analysis by Ref. [74], which indeed also favours a non-zero value for m_s (see Fig. 6). It is of interest to note that the EE best-fit residuals in this multipole range are also very similar to those obtained in very recent analyses against ACT data carried out in the context of models with dark energy at early times [88, 90, 91]. Even in that framework, the mild tension between *Planck* and ACT data on intermediate multipoles translates into hints for new physics beyond ΛCDM, namely into a slight preference for a non-zero early dark energy component [90, 91]. Our results, as well as theirs, explicitly demonstrate the importance of examining predictions coming from
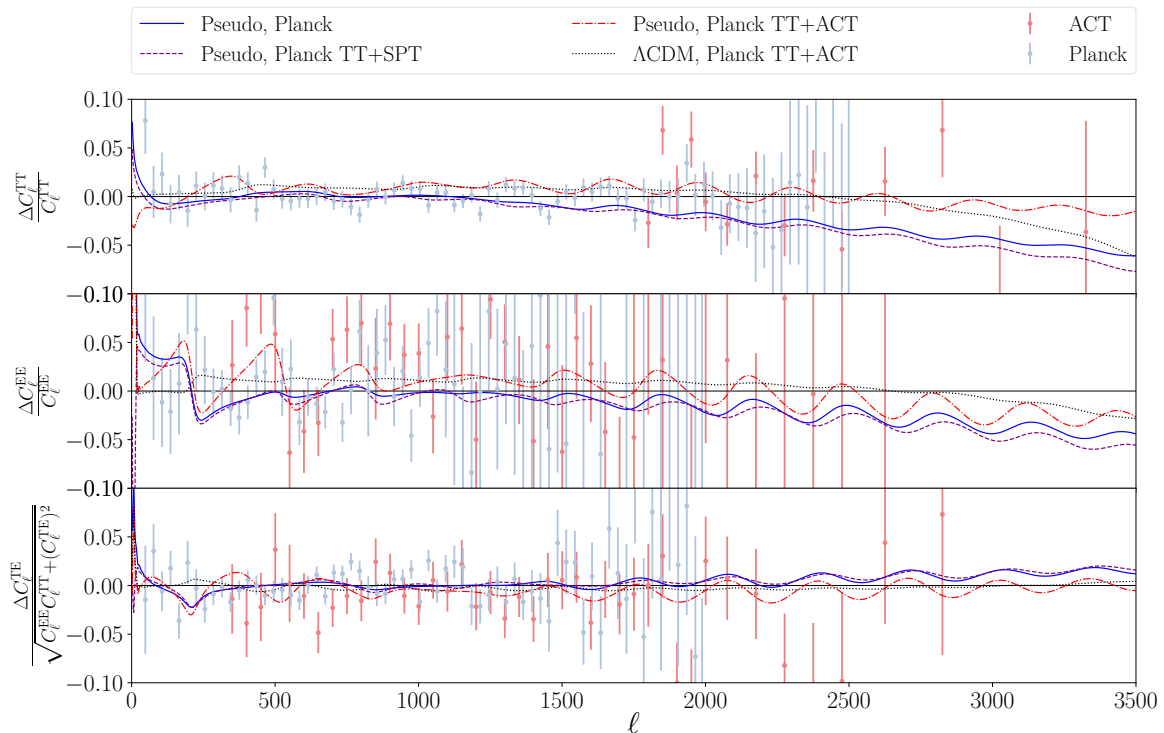
Figure 2. Residuals in the (lensed) CMB TT, EE and TE power spectrum with respect to the *Planck*-only ΛCDM best-fit. We also show *Planck* and ACT data-points and error bars.

different CMB data combinations, especially within non-trivial extensions of the ΛCDM scenario. The oscillation pattern in the best-fit *Planck* TT+ACT spectra around $\ell \sim 500$ reflects the trend of ACT data-points. The fact that the latter ones are in mild tension with *Planck* data implies that the ΛCDM best-fit from *Planck* does not necessarily provide a good fit to ACT data with respect to alternative scenarios, such as the pseudoscalar model under study. We will discuss in detail sources and implications of the slight inconsistency between *Planck* and ACT in Section 5, also thanks to a series of additional MCMC analyses.

4.4 Implications for the CMB lensing anomaly

Let us now focus on the lensing anomaly in *Planck* data, and on studying the robustness of the constraints in the pseudoscalar model when marginalizing over the lensing information in *Planck* data. As described in the Introduction, this is done by introducing and varying two additional parameters, $A_{\mathrm{L}}^{\mathrm{TTTEEE}}$ and $A_{\mathrm{L}}^{\phi\phi}$, as in Refs. [87, 92–94]. The results are shown in Fig. 3 and in the second column of Tab. 1, from which we note that the lensing anomaly is not relaxed and that the tight constraint on the sterile neutrino mass is not alleviated by the introduction of the two extra parameters. As in the ΛCDM framework, in this set-up there is no growth tension, due to the anti-correlation of S_8 with the lensing parameters. Moreover, Fig. 3 clearly shows that the introduction of $A_{\mathrm{L}}^{\mathrm{TTTEEE}}$ and $A_{\mathrm{L}}^{\phi\phi}$ introduces new degeneracies in the parameter space, resulting in higher values for both n_s and H_0. Since both of them are positively correlated with ΔN_{eff}, the tight bound on the latter is relaxed, resulting in $\Delta N_{\mathrm{eff}} = 0.37^{+0.17}_{-0.25}$, i.e. a mild preference for a non-zero value of the number of additional
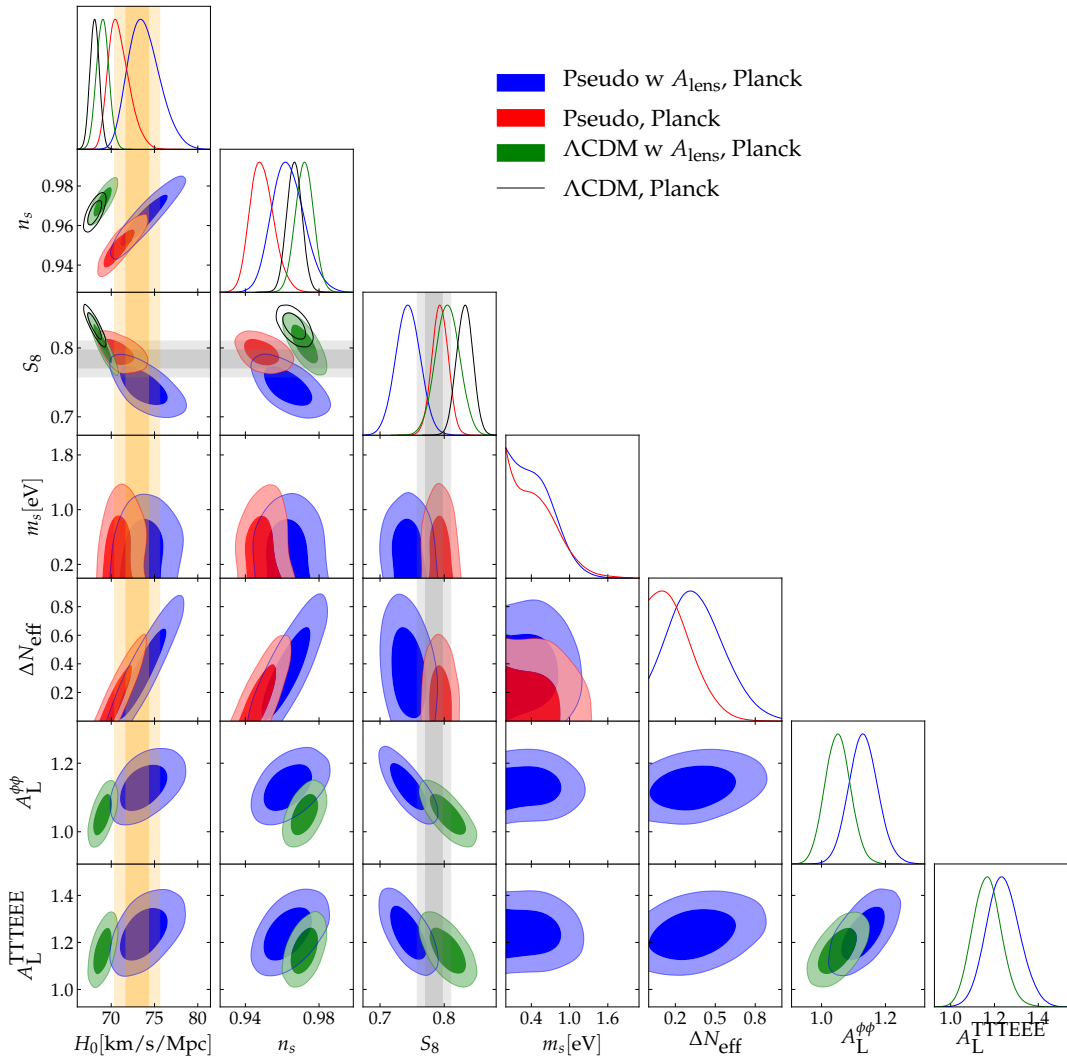
Figure 3. Posterior distributions of the cosmological parameters in the ΛCDM and pseudoscalar (Pseudo) model tested with *Planck* data, with and without marginalizing over the gravitational lensing information. The orange and gray bands represent the direct measurements (1 σ and 2 σ confidence regions) of H_0 and S_8, from cosmic distance ladder [9] and weak lensing data [18], respectively.

relativistic species. In other words, the presence of the two additional lensing parameters allows us to find higher values along the well-known H_0–ΔN_{eff} degeneracy direction without a significant impact on the CMB observables.

Let us now recall that within ΛCDM the CMB lensing anomaly is characterized by two different aspects: (i) the anomalous value of the observed lensing amplitude parameter, discrepant with the model prediction; (ii) the fact that only $A_{\text{L}}^{\text{TTTEEE}}$ is anomalous, while $A_{\text{L}}^{\phi\phi}$ is compatible with 1, implying that the effect on the TT-TE-EE spectra that seems to be due to an extra-source of gravitational lensing cannot be attributed to actual gravitational lensing. From Fig. 3 one can notice that in the pseudoscalar model both the lensing parameters depart from 1, indicating that in such a scenario the condition (ii) is not verified. Namely, the extra-smoothing of the peaks is still present but might be attributed to actual lensing. Nonetheless,

this result should be taken with great care, given that $A_L^{\phi\phi}$ is again fully compatible with 1 as soon as one adds to the analysis complementary low-redshift data from BAO and SnIa, as we will show in the next Subsection.
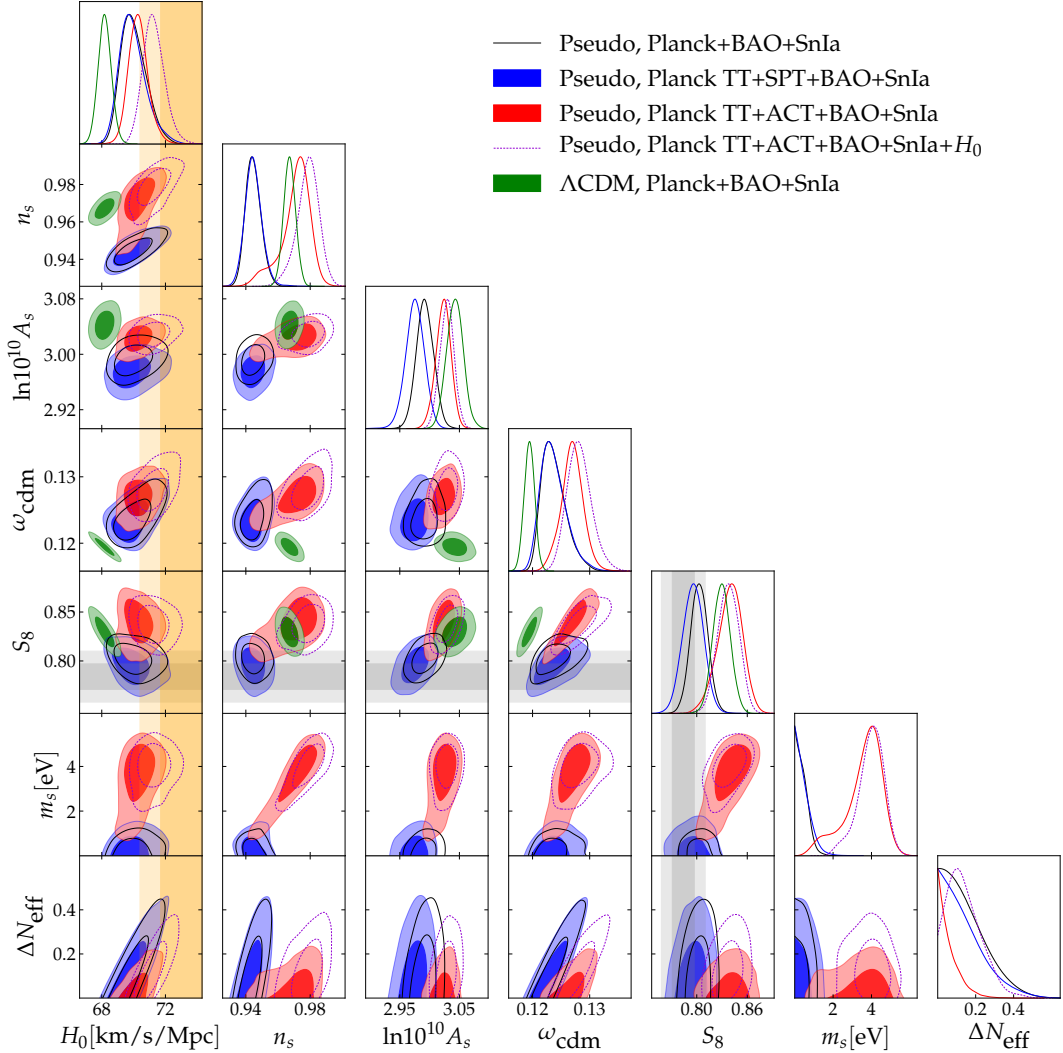
4.5 Impact of additional low-redshift data

Figure 4. Posterior distributions of the cosmological parameters in the ΛCDM and pseudoscalar (Pseudo) model for different data-sets. The orange and gray bands represent the direct measurements (1 σ and 2 σ confidence regions) of H_0 and S_8, from cosmic distance ladder [9] and weak lensing observations [18], respectively.

We now examine the impact of adding low-redshift data from BAO and SnIa to the various CMB set-ups presented in the previous Subsections. In Fig. 4 we show how the limits on the pseudoscalar model displayed in Fig. 1 are affected by the addition of BAO and SnIa data, whereas in Fig. 5 we show the impact of such low-redshift probes on the predictions within the pseudoscalar scenario when marginalizing over the lensing parameters as we did in Subsection 4.4. The corresponding mean values and ±1σ C.L. are reported
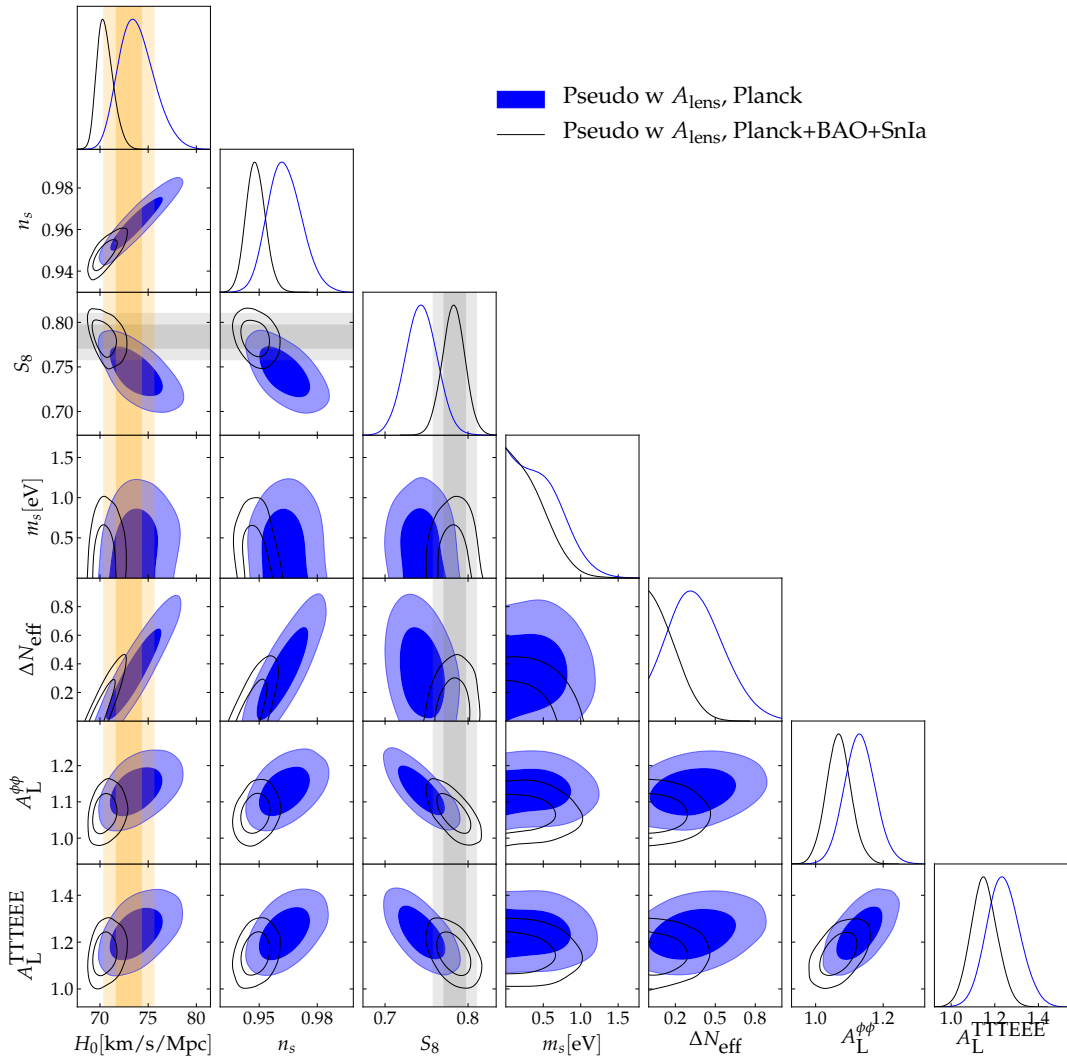
Figure 5. Posterior distributions of the cosmological parameters in the pseudoscalar (Pseudo) model tested with *Planck* data marginalizing over the gravitational lensing information, with and without the addition of BAO and SnIa. The orange and gray bands represent the direct measurements (1 σ and 2 σ confidence regions) of H_0 and S_8, from cosmic distance ladder [9] and weak lensing observations [18], respectively.

in Tab. 2. The addition of BAO+SnIa data does not significantly shift the posteriors of the cosmological parameters. Concerning the *Planck* analysis, our results are in excellent agreement with those from Ref. [74], with minor differences due to a slightly different choice for the BAO data-set. In the *Planck* TT+SPT analysis, the additional constraining power coming from low-redshift data further tightens the limits on the m_s and $\Delta N_{\rm eff}$ parameters. In the *Planck* TT+ACT case, the preference for a non-zero value for m_s is not affected by the addition of low-redshift data, although the global fit is slightly degraded ($\Delta \chi^2 \simeq 6$ instead of $\Delta \chi^2 \simeq 3$, compared to ΛCDM) with respect to the case without BAO+SnIa. Both in Fig. 4 and Tab. 2, we also report the results of a *Planck* TT+ACT+BAO+SnIa analysis carried out adopting an effective calibration prior on the absolute magnitude (M_B) of SnIa [109, 110] that corresponds to the direct determination of $H_0 = 73.04^{+1.04}_{-1.04}$ km/s/Mpc

from the SH0ES Collaboration [111][7]. By comparing the full red and empty purple contours in Fig. 4, we note that the preference for a larger value of n_s is cleaner, with a clear peak around $n_s = 0.9786^{+0.0076}_{-0.0055}$. The tails at low values of both n_s and m_s disappear, and there is now a mild hint for a non-zero $\Delta N_{\rm eff} = 0.14^{+0.05}_{-0.13}$, due to the well-known positive correlation of the latter with the Hubble parameter. The corresponding value of $H_0 = 71.3^{+0.6}_{-0.8}$ km/s/Mpc is in good agreement with its local measurement. We obtain indeed a total $\Delta\chi^2 \simeq -10$ with respect to the ΛCDM model and, according to the Akaike Information Criterion [112] (AIC), this is the only analysis discussed so far where the pseudoscalar model is preferred over ΛCDM (see Tab. 7). As anticipated, in Fig. 5 we show that, although in the *Planck*-only analysis of the pseudoscalar model both the lensing parameters are anomalous (see Sec. 4.4), the addition of BAO+SnIa data shifts the posterior distributions of $A_{\rm L}^{\phi\phi}$ towards the ΛCDM prediction, such that $A_{\rm L}^{\phi\phi}$ is again fully compatible with 1. Moreover, the addition of low-redshift probes has the effect of reducing the parameter space opened by the introduction of free $A_{\rm L}^{\rm TTTEEE}$ and $A_{\rm L}^{\phi\phi}$ in the CMB-only analysis, such that the prediction of n_s, H_0 and $\Delta N_{\rm eff}$ are now close to the one obtained in the *Planck*+BAO+SnIa case (see also Tab. 2). The price to pay for the changes in the parameter values induced to accommodate BAO+SnIa data, is a slight degradation of the fit to *Planck* high-ℓ TT data ($\Delta\chi^2 \simeq 10$ instead of $\Delta\chi^2 \simeq 7$, compared to ΛCDM).

5 Planck vs ACT: a deeper look

As explained in the previous Section, our results explicitly demonstrate that the approximate consistency of cosmological parameters inferred from *Planck* and ACT in the ΛCDM framework [82] does not necessarily imply their consistency in more complex models. In fact, the apparent (mild) tension between *Planck* and ACT data in the EE and TE spectra at around $\ell \sim 500$ could have non-trivial implications in extended models compared to ΛCDM, as it was also pointed out very recently within scenarios featuring dark energy at early times [90, 91]. In this Section, we further investigate the source of the tension between *Planck* and ACT polarization data, that in the model under study is directly responsible for the preference for a non-zero sterile neutrino mass in the joint *Planck* TT+ACT analysis. To that aim, we

---

[7] https://github.com/valerio-marra/CalPriorSNIa.

Parameter	Pseudo vs CMB + BAO + SnIa				
	Planck	*Planck* w. $A_{\rm lens}$	*Planck* TT+SPT	*Planck* TT+ACT	$+H_0$
$100\,\omega_b$	$2.259^{+0.022}_{-0.019}$	$2.276^{+0.023}_{-0.020}$	$2.269^{+0.032}_{-0.023}$	$2.209^{+0.018}_{-0.021}$	$2.225^{+0.018}_{-0.020}$
$\omega_{\rm cdm}$	$0.1237^{+0.0015}_{-0.0025}$	$0.1225^{+0.0016}_{-0.0026}$	$0.1236^{+0.0016}_{-0.0027}$	$0.1269^{+0.0020}_{-0.0018}$	$0.1282^{+0.0019}_{-0.0025}$
$100\,\theta_s$	$1.04520^{+0.00037}_{-0.00037}$	$1.04540^{+0.00036}_{-0.00037}$	$1.04490^{+0.00043}_{-0.00047}$	$1.04660^{+0.00051}_{-0.00041}$	$1.04680^{+0.00043}_{-0.00042}$
$\ln 10^{10} A_s$	$2.992^{+0.014}_{-0.015}$	$2.971^{+0.018}_{-0.016}$	$2.976^{+0.016}_{-0.016}$	$3.023^{+0.013}_{-0.012}$	$3.025^{+0.011}_{-0.012}$
n_s	$0.9444^{+0.0043}_{-0.0053}$	$0.9482^{+0.0047}_{-0.0053}$	$0.9448^{+0.0049}_{-0.0055}$	$0.971^{+0.011}_{-0.006}$	$0.9786^{+0.0076}_{-0.0055}$
$\tau_{\rm reio}$	$0.0556^{+0.0069}_{-0.0072}$	$0.0480^{+0.0085}_{-0.0074}$	$0.0492^{+0.0080}_{-0.0074}$	$0.0520^{+0.0056}_{-0.0058}$	$0.0532^{+0.0052}_{-0.0062}$
m_s [eV]	< 1.0	< 0.8	< 1.3	$3.6^{+1.1}_{-0.5}$	$3.992^{+0.77}_{-0.55}$
$\Delta N_{\rm eff}$	< 0.36	< 0.38	< 0.37	< 0.18	$0.14^{+0.05}_{-0.13}$
$A_{\rm L}^{\phi\phi}$		$1.069^{+0.036}_{-0.037}$			
$A_{\rm L}^{\rm TTTEEE}$		$1.151^{+0.060}_{-0.064}$			
H_0 [km/s/Mpc]	$70.0^{+0.7}_{-0.9}$	$70.6^{+0.7}_{-1.0}$	$69.7^{+0.7}_{-1.0}$	$70.3^{+0.6}_{-0.7}$	$71.3^{+0.6}_{-0.8}$
S_8	$0.803^{+0.010}_{-0.011}$	$0.783^{+0.014}_{-0.014}$	$0.796^{+0.013}_{-0.013}$	$0.839^{+0.017}_{-0.013}$	$0.838^{+0.014}_{-0.013}$

Table 2. The mean $\pm 1\,\sigma$ error ($2\,\sigma$ in the case of upper bounds) of the cosmological parameters from CMB experiments in the pseudoscalar model.
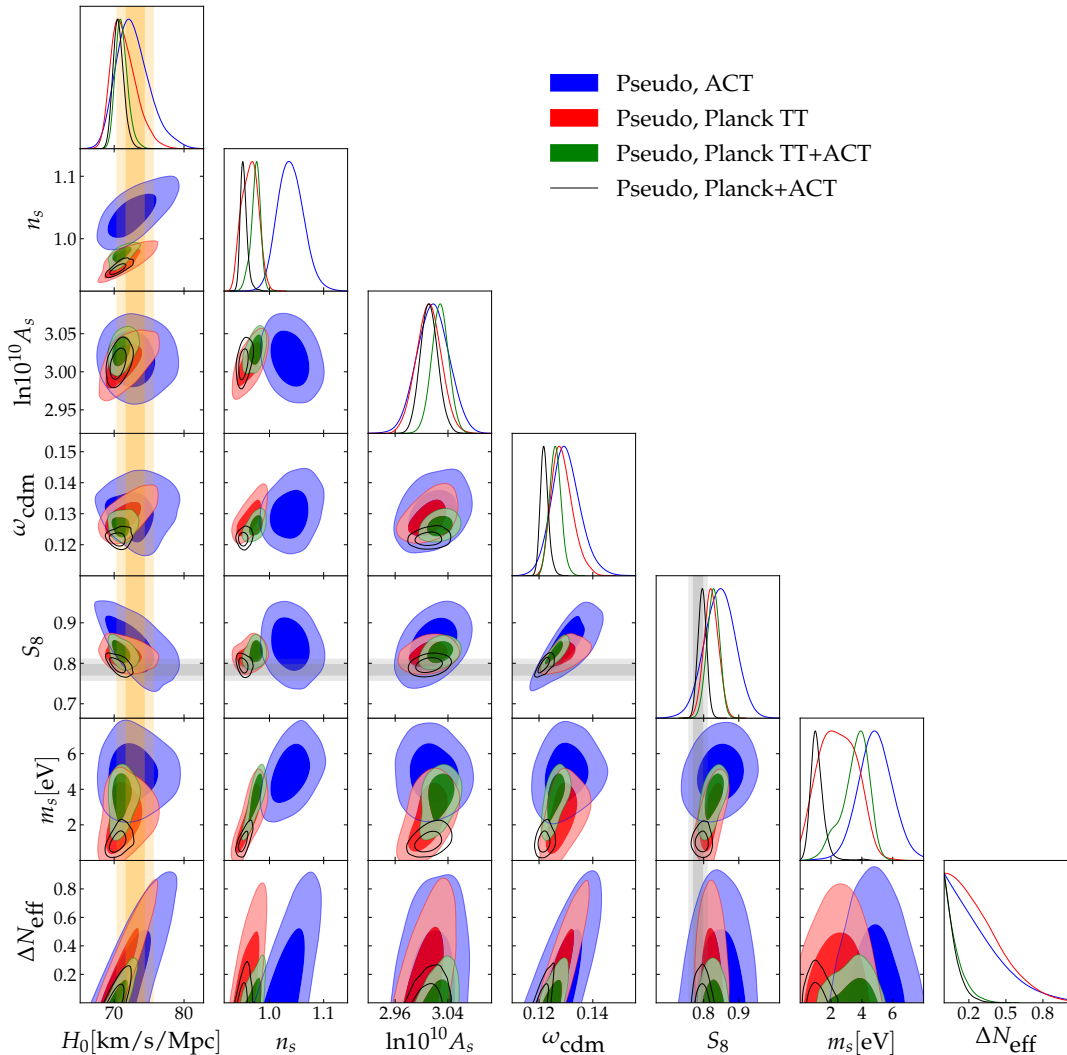
Figure 6. Posterior distributions of the cosmological parameters in the pseudoscalar (Pseudo) model for different data-sets. The orange and gray bands represent the direct measurements (1 σ and 2 σ confidence regions) of H_0 and S_8, from cosmic distance ladder [9] and weak lensing observations [18], respectively.

performed a set of additional MCMC runs, summarized in Fig. 6 and Tab. 3. We tested the pseudoscalar model against ACT data alone, *Planck* low-ℓ + high-ℓ TT data as in Ref. [74], and the combination of ACT data with the full data-set from *Planck*. Hereafter, we label them as ACT, *Planck* TT and *Planck*+ACT, respectively. Let us note that the pseudoscalar model provides a better fit with respect to ΛCDM in the ACT-only analysis ($\Delta\chi^2 \simeq -5$), and appears also to be mildly favoured according to the AIC, although this preference disappears as soon as BAO+SnIa are added to the analysis (see Tabs. 6 and 7). In Sec. 4.2 we pointed out that the preference for a non-zero m_s is driven by the preference for higher values of n_s from ACT data, compared to *Planck* and SPT, as already discussed by the ACT Collaboration in the ΛCDM context [82]. Indeed, the relatively low constraining power from ACT on large angular scales results in a strong anti-correlation between ω_b and n_s. Hence, a lower
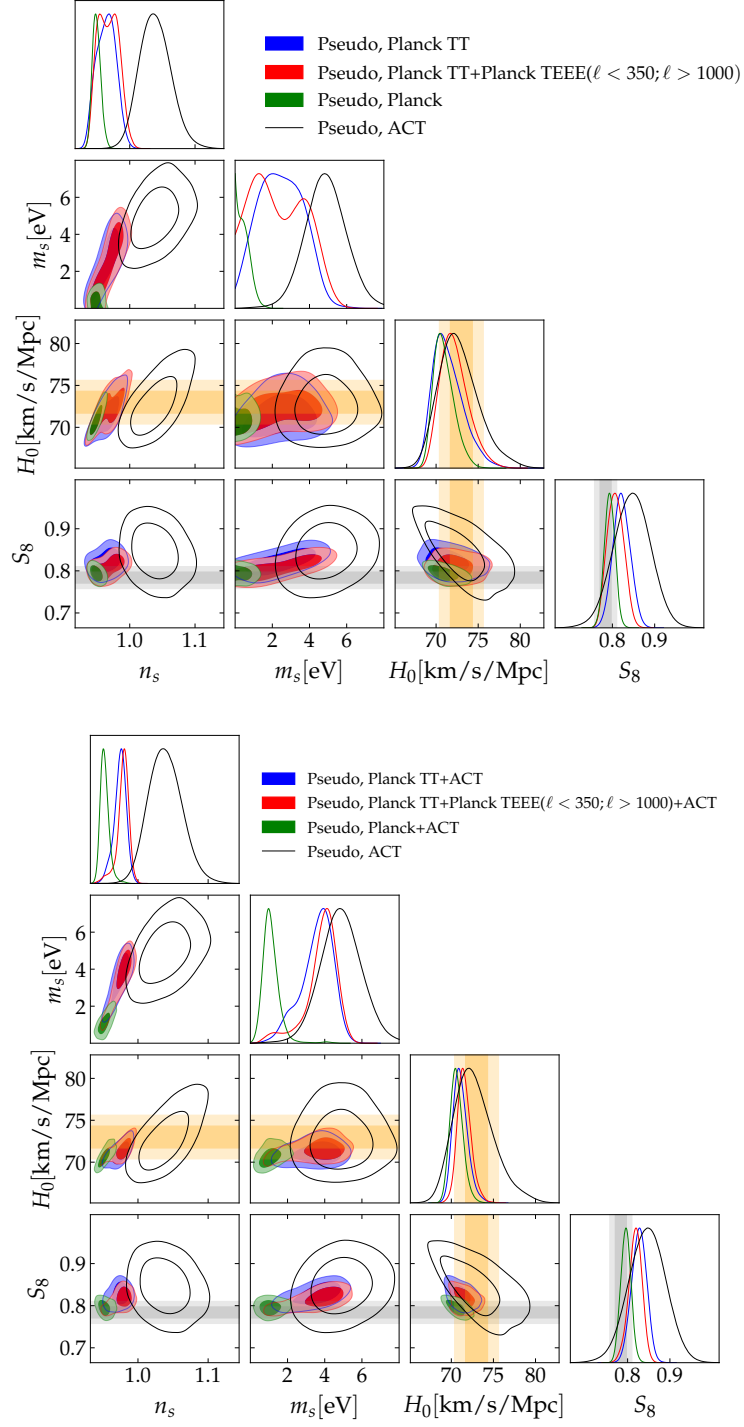
Figure 7. Posterior distributions of the cosmological parameters in the pseudoscalar (Pseudo) model for different subsets of *Planck* TE-EE data with and without the inclusion of ACT. The orange and gray bands represent the direct measurements (1 σ and 2 σ confidence regions) of H_0 and S_8, from cosmic distance ladder [9] and weak lensing observations [18], respectively.

value of the baryon density, which damps the small-scale power spectrum, can be partially compensated by a higher value of the spectral index which tilts the spectrum to restore the small-scale power [82]. Within that degeneracy direction, ACT data favour a lower ω_b and a higher n_s, with respect to *Planck*. As one can see from Fig. 6 and the first two columns of Tab. 3, ACT data alone prefer a value of n_s greater than one even in the pseudoscalar scenario. In light of these considerations, our choice to consider the joint *Planck* TT+ACT as our reference data combination, as we did in Sec. 4.2, appears the most natural one, since in this data-set the posterior of n_s is shifted towards values lower than one. Strikingly, this shift only marginally affects the posterior of m_s, so that a non-zero mass is still preferred. Let us also notice that neither ACT nor *Planck* TT data alone put very tight limits on $\Delta N_{\rm eff}$, whereas their joint analysis makes the constraint on this parameter very stringent, due to the broken degeneracy in the $\Delta N_{\rm eff} - n_s$ plane. From Fig. 6 we can also note that the posterior distributions of the *Planck* TT analysis agree very well with the results from Ref. [74], and are always in good agreement with those from ACT-only, ensuring the statistical consistency of the joint *Planck* TT+ACT analysis. As we also stressed in Sec. 4.3, the predictions of our reference analysis are indeed very similar to those from *Planck* TT data only, besides featuring narrower posteriors.

Let us now examine the *Planck*+ACT results. As expected, the posteriors of m_s and n_s sit midway between the ones obtained from individually considering ACT or *Planck*, predicting a lower, but still non-zero value for the sterile mass, i.e. $m_s = 1.1^{+0.3}_{-0.5}$ eV (68% C.L.), and a lower S_8 value. There is of course a strong degradation of the global fit with respect to ΛCDM ($\Delta\chi^2 \simeq 16$) driven indeed by a poor fit to both ACT and *Planck* data. However, these latter results must be considered only as a proof-of-principle, given that such a data combination is not fully statistically consistent. As one can notice by comparing the first column of Tab. 1 with the first column of Tab. 3, the two data-sets predict values for n_s and m_s which are in disagreement at $\gtrsim 3\sigma$.

In order to identify which subset of *Planck* TE-EE data drives the tension with ACT, making the combination of the full *Planck* data-set with ACT statistically inconsistent, we performed a further set of analyses where we imposed different cuts in the multipole range of *Planck* TE-EE data, as shown in Fig. 7 (see also App. B). The results reported in Fig. 7 clearly illustrate that it is possible to find a subset of *Planck* polarization data that, when combined with *Planck* TT, is in statistical agreement with ACT. From the upper panel of Fig. 7 we note indeed that when we "restrict" *Planck* TE-EE data by excluding multipoles between $350 < \ell < 1000$, we obtain parameter bounds in agreement at approximately $1\,\sigma$ with ACT predictions. Hence, the tight constraint on n_s, inconsistent with the values favoured by ACT, is driven by *Planck* TE-EE data in that multipole range. In the lower panel of Fig. 7 we report the results of the same "restricted" *Planck* analysis, but in combination with ACT.

Both analyses are fully statistically consistent, and the corresponding contours in excellent agreement with those from *Planck* TT+ACT. Therefore, we can conclude that the possibility of a non-zero sterile neutrino mass is primarily excluded by *Planck* polarization data in the multipole range between $350 \lesssim \ell \lesssim 1000$, also in accordance from what one can intuitively guess from Fig. 2. The range of TE-EE multipoles where ACT and *Planck* residuals significantly differ from each other is indeed $350 \lesssim \ell \lesssim 1000$, and on such intermediate multipoles the *Planck* TT+ACT best-fit pseudoscalar model features the enhanced oscillation pattern with respect to ΛCDM that we discussed in detail in Sec. 4.3. Intriguingly, that interval of multipoles plays a crucial role also in the detection of a non-zero fraction of early dark energy when ACT data are taken into account [90, 91]. Future work including higher

Parameter	Pseudoscalar model			
	ACT	+BAO+SnIa	*Planck*+ACT	+BAO+SnIa
$100\,\omega_b$	$2.185^{+0.035}_{-0.037}$	$2.175^{+0.032}_{-0.035}$	$2.239^{+0.017}_{-0.020}$	$2.238^{+0.018}_{-0.019}$
$\omega_{\rm cdm}$	$0.1301^{+0.0049}_{-0.0059}$	$0.1311^{+0.0024}_{-0.0042}$	$0.1220^{+0.0013}_{-0.0018}$	$0.1226^{+0.0011}_{-0.0015}$
$100\,\theta_s$	$1.04800^{+0.00081}_{-0.00081}$	$1.04770^{+0.00079}_{-0.00074}$	$1.04600^{+0.00037}_{-0.00046}$	$1.04580^{+0.00033}_{-0.00038}$
$\ln 10^{10} A_s$	$3.017^{+0.024}_{-0.026}$	$3.014^{+0.025}_{-0.023}$	$3.012^{+0.013}_{-0.014}$	$3.005^{+0.012}_{-0.012}$
n_s	$1.039^{+0.022}_{-0.026}$	$1.022^{+0.019}_{-0.021}$	$0.9527^{+0.0047}_{-0.0077}$	$0.9475^{+0.0038}_{-0.0050}$
$\tau_{\rm reio}$	$0.06^{+0.01}_{-0.01}$	$0.055^{+0.010}_{-0.009}$	$0.0582^{+0.0059}_{-0.0065}$	$0.0558^{+0.0056}_{-0.0060}$
m_s [eV]	$4.9^{+1.1}_{-1.2}$	$4.6^{+1.2}_{-1.1}$	$1.1^{+0.3}_{-0.5}$	$0.9^{+0.3}_{-0.4}$
$\Delta N_{\rm eff}$	< 0.75	< 0.47	< 0.21	< 0.16
H_0 [km/s/Mpc]	$72.7^{+2.0}_{-2.8}$	$70.6^{+0.8}_{-1.2}$	$70.6^{+0.7}_{-0.9}$	$69.8^{+0.5}_{-0.6}$
S_8	$0.846^{+0.045}_{-0.044}$	$0.873^{+0.021}_{-0.021}$	$0.796^{+0.012}_{-0.013}$	$0.806^{+0.010}_{-0.010}$

Table 3. The mean $\pm 1\,\sigma$ error ($2\,\sigma$ in the case of upper bounds) of the cosmological parameters from CMB experiments in the pseudoscalar model.

precision data from current and upcoming CMB ground-based experiments will be crucial to test these results, and to understand whether the mild tension between *Planck* and ACT is due to some unaccounted systematics or a statistical fluke.

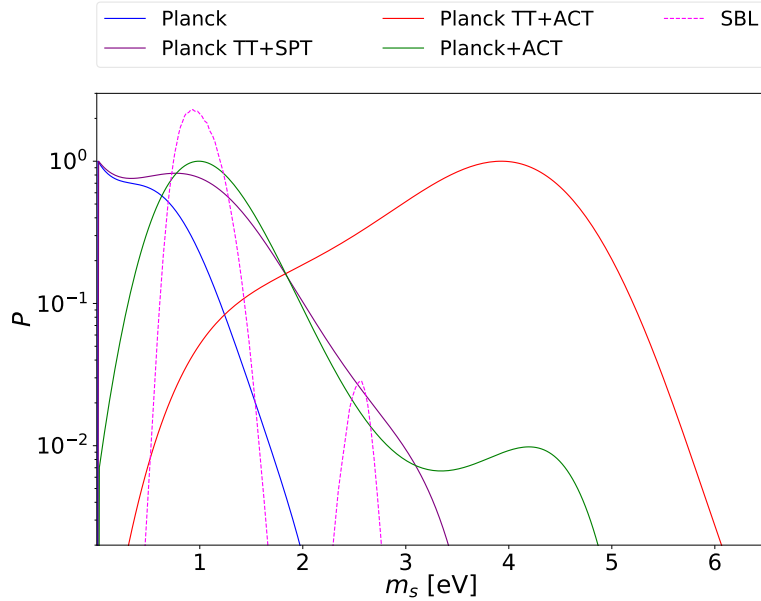# 6 Comparison with SBL neutrino oscillation experiments

Figure 8. Marginalized 1-D posterior distributions for the sterile neutrino mass, in the pseudoscalar model, from the cosmological analyses performed in this work (solid lines) and from SBL data (dashed line). See Sec. 6 for a detailed description of the latter ones.

As discussed in the Introduction, SBL neutrino oscillation anomalies may be explained by the existence of a sterile neutrino at the eV mass scale (see the recent reviews in Refs. [38, 47, 48]). However, the tension between appearance and disappearance SBL neutrino oscillation data in the framework of 3+1 active-sterile neutrino mixing [50–52] does not allow us to obtain a global SBL fit. Moreover, the reactor antineutrino anomaly has been

revised and reduced recently [53, 54]. On the other hand, the Gallium anomaly has been reinforced by the recent results of the BEST experiment [56], but it is in tension with the reactor data [54], with the negative results of the DANSS [113], PROSPECT [114], and STEREO [115] experiments [57], and with the solar bound [54, 58, 116]. Considering the SBL $\nu_\mu \to \nu_e$ appearance channel, the MiniBooNE low-energy anomaly [40, 41] has been recently disfavored by the results of the MicroBooNE experiment [59–61] (see, however, the caveats in Ref. [62] and the possible interpretation of the MicroBooNE data in terms of SBL ν_e disappearance in Ref. [63]). Only the LSND excess in the $\bar{\nu}_\mu \to \bar{\nu}_e$ appearance channel [39] has not been excluded by other experiments so far (it will be soon under investigation in the SBN [117] and JSNS^2 [118] experiments). Therefore, we consider the LSND excess [39] taking into account the constraints on the sterile neutrino mass given by the negative results of the BNL-E776 [119], KARMEN [120], NOMAD [121], ICARUS [122] and OPERA [123] $\nu_\mu \to \nu_e$ appearance experiments. The Bayesian posterior given by the combined fit of the data of these experiments is shown by the dashed line in Fig. 8. One can see that there is a main peak around $m_s \approx 1\,\mathrm{eV}$ and a secondary peak around $m_s \approx 2.5\,\mathrm{eV}$. There is a clear compatibility between these values of m_s and the cosmological indications in the pseudoscalar model.

7 Conclusions

In this work we have employed a whole host of up-to-date cosmological data, both at the background and at the linear perturbation level, to test the cosmological scenario first proposed in Ref. [70] and more recently studied in Refs. [72–74], where an additional light sterile neutrino species is allowed to self-interact, through a new pseudoscalar mediator. This scenario naturally predicts a value of H_0 consistent with its local measurements, and it provides a good fit to CMB data without spoiling LSS bounds on the neutrino mass nor worsening the S_8 tension with respect to the ΛCDM model. While being slightly favoured by *Planck* temperature only data [73], a non-zero sterile neutrino mass – compatible with the range suggested to explain SBL anomalies – is however severely constrained by the addition of high-ℓ polarization data, as already pointed out in Ref. [74].

Given the availability of ground-based CMB maps with better angular resolution than *Planck* on intermediate and high multipoles, our goal was to test the robustness of the tight limits on the sterile neutrino properties from Ref. [74], and at the same time evaluate the impact of the pseudoscalar model on the CMB lensing anomaly, which affects high-ℓ *Planck* data. To this end, we have expanded previous analyses as follows: (i) showing the impact of marginalizing over the CMB lensing amplitude in *Planck* data; (ii) replacing *Planck* high-ℓ polarization data with those from two ground-based CMB surveys, i.e. SPT [80] and ACT [82]. In all our analyses we have found that the model under study is able to resolve the Hubble tension without worsening the growth tension compared to the ΛCDM model, while we see no impact on the CMB lensing anomaly. We have also shown that using additional low-redshift data from BAO and uncalibrated SnIa does not qualitatively affect the constraints, besides a general strengthening of the credible regions. Both when considering a free lensing amplitude and in the *Planck* TT+SPT analysis, we have demonstrated that the strong bound on the sterile neutrino mass is not relaxed.

Things dramatically change when the model is confronted against ACT data. This data-set, both alone and in combination with *Planck*, shows indeed a $\gtrsim 3\,\sigma$ preference for a non-zero sterile neutrino mass in the eV range. In particular, in the *Planck* TT+ACT analysis we find $m_s = 3.6^{+1.1}_{-0.6}$ eV (68% C.L.). We have shown that this is due to the positive

correlation with the high value of the tilt of the primordial power spectrum n_s favoured by ACT – even within ΛCDM – compared to *Planck* and SPT. The pseudoscalar model appears indeed to provide a better fit to ACT data with respect to ΛCDM ($\Delta\chi^2 \simeq -5$). Interestingly, we have found that the values of n_s and m_s inferred from the entire *Planck* data-set differ at $\gtrsim 3\sigma$ from those predicted by ACT alone, making a full *Planck*+ACT analysis statistically inconsistent. We have thus carried out a further set of studies aimed at identifying which subset of *Planck* polarization data is responsible for this tension. We have explicitly shown that the values of n_s and m_s favoured by multipoles higher (lower) than 1000 (350) from *Planck* TE-EE data are still consistent with ACT predictions, meaning that the severe constraint on the sterile neutrino mass is driven by *Planck* TE-EE data in the multipole range $350 \lesssim \ell \lesssim 1000$. The slight discrepancy between *Planck* and ACT on intermediate multipoles does not have a major impact within the ΛCDM model [82]. It can however lead to highly non-trivial results not only within the self-interacting sterile neutrino scenario studied here, but also in other alternative models that could resolve to the Hubble tension, such as early dark energy scenarios [90, 91, 124, 125]. It will thus be crucial to establish whether the discrepancy is due to yet unaccounted systematics or a statistical fluke either in *Planck* or in ACT data. Our results highlight the importance of testing non-trivial extensions of the ΛCDM model against upcoming, more accurate measurements of the CMB spectra from future surveys, such as CMB-S4 [126] or the Simons Observatory [127], as well as new data releases from both ACT and SPT [85].

Acknowledgments

	Individual χ^2: ΛCDM vs CMB					
	Planck	*Planck* w. $A_{\rm lens}$	*Planck* TT+SPT	*Planck* TT+ACT	ACT	*Planck*+ACT
Planck high$-\ell$ TT,TE,EE	2346.5	2340.1	-	-	-	2348.8
Planck high$-\ell$ TT	-	-	762.0	764.6	-	-
Planck low$-\ell$ EE	395.7	395.7	395.7	396.1	-	396.2
Planck low$-\ell$ TT	22.9	21.5	22.7	22.3	-	22.2
Planck lensing	9.0	8.7	-	9.1	-	9.1
SPT high$-\ell$ TE,EE	-	-	146.8	-	-	-
SPT lensing	-	-	5.7	-	-	-
ACT DR4	-	-	-	-	280.1	-
ACT DR4 ($\ell_{\rm TT} > 1800$)	-	-	-	239.1	-	240.7
total	2774.1	2766.0	1332.9	1431.2	280.1	3017.0

Table 4. Best-fit χ^2 per experiment (and total) from our CMB analyses in the ΛCDM model.

	Individual χ^2: ΛCDM vs CMB + BAO + SnIa						
	Planck	*Planck* w. $A_{\rm lens}$	*Planck* TT+SPT	*Planck* TT+ACT	+H_0	ACT	*Planck*+ACT
Pantheon SnIa	1026.9	1026.8	1026.9	1026.9	1027.2	1027.0	1026.9
BAO+FS BOSS DR12	6.2	6.3	6.1	6.2	7.3	6.5	6.4
BAO BOSS low−z	1.9	2.1	2.0	1.9	2.6	1.8	1.7
eBOSS DR14 Lyman−α	4.5	4.4	4.5	4.5	4.3	4.9	4.6
Planck high−ℓ TT,TE,EE	2346.5	2340.1	-	-	-	-	2349.4
Planck high−ℓ TT	-	-	763.2	765.7	766.3	-	-
Planck low−ℓ EE	395.8	395.7	395.7	395.7	396.4	-	396.6
Planck low−ℓ TT	22.8	22.2	22.5	22.1	22.0	-	22.2
Planck lensing	8.9	9.1	-	9.1	9.0	-	9.3
SPT high−ℓ TE,EE	-	-	146.6	-	-	-	-
SPT lensing	-	-	5.5	-	-	-	-
ACT DR4	-	-	-	-	-	280.3	-
ACT DR4 ($\ell_{\rm TT} > 1800$)	-	-	-	238.4	238.5	-	240.0
M_B Prior (SH_0ES 2021)	-	-	-	-	21.2	-	-
total	3813.5	3806.7	2373.0	2470.5	2494.8	1320.5	4057.1

Table 5. Best-fit χ^2 per experiment (and total) from our CMB analyses in combination with BAO and SnIa in the ΛCDM model.

	Individual χ^2: Pseudo vs CMB					
	Planck	*Planck* w. $A_{\rm lens}$	*Planck* TT+SPT	*Planck* TT+ACT	ACT	*Planck*+ACT
Planck high−ℓ TT,TE,EE	2356.3	2347.3	-	-	-	2367.7
Planck high−ℓ TT	-	-	769.6	773.2	-	-
Planck low−ℓ EE	396.1	395.7	395.9	396.3	-	396.7
Planck low−ℓ TT	24.9	22.0	24.0	21.2	-	24.0
Planck lensing	9.0	8.2	-	10.8	-	9.0
SPT high−ℓ TE,EE	-	-	149.4	-	-	-
SPT lensing	-	-	5.1	-	-	-
ACT DR4	-	-	-	-	274.8	-
ACT DR4 ($\ell_{\rm TT} > 1800$)	-	-	-	233.2	-	237.0
total	2786.3	2773.2	1344.0	1434.7	274.8	3034.4
total $\Delta\chi^2$	12.2	7.2	11.1	3.5	-5.3	17.4
ΔAIC	16.2	11.2	15.1	7.5	-1.3	21.4

Table 6. Best-fit χ^2 per experiment (and total) from our CMB analyses in the pseudoscalar model. Per each run, we also report the corresponding $\Delta\chi^2 \equiv \chi^2_{\rm min,pseudo}$-$\chi^2_{\rm min,\Lambda CDM}$. In order to determine if the pseudoscalar model is favoured by the data in the analyses considered, we compute the AIC relative to that of ΛCDM (ΔAIC). Negative values of the latter correspond to a preference for the pseudoscalar model over ΛCDM.

A Best-fit parameter values and χ^2 per experiment

In Tabs. 4, 5 and in Tabs. 6, 7 we report the $\chi^2_{\rm min}$'s obtained respectively for the most significant ΛCDM and pseudoscalar analyses considered. In order to determine if the pseudoscalar model is favoured by the data in the analyses performed, we computed the AIC [112] relative to that of ΛCDM as ΔAIC = $2(\mathcal{N}_{\rm pseudo} - \mathcal{N}_{\Lambda CDM}) + \Delta\chi^2$, where $\Delta\chi^2 \equiv \chi^2_{\rm min,pseudo}$-$\chi^2_{\rm min,\Lambda CDM}$ while $\mathcal{N}_{\rm pseudo}$ and $\mathcal{N}_{\Lambda CDM}$ are the number of free parameters in the pseudoscalar and ΛCDM model respectively. The pseudoscalar model is favoured over ΛCDM when negative values of ΔAIC are found. In Tabs. 8 and 9 we also report the best-fit parameter values.

B Additional results with different subsets of Planck polarization data

In Sec. 5, we stated that the bound on the sterile neutrino mass comes from *Planck* TE-EE data from $350 \lesssim \ell \lesssim 1000$. In this Appendix we discuss some of the additional analyses

	Individual χ^2: Pseudo vs CMB + BAO + SnIa						
	Planck	*Planck* w. $A_{\rm lens}$	*Planck* TT+SPT	*Planck* TT+ACT	$+H_0$	ACT	*Planck*+ACT
Pantheon SnIa	1026.9	1026.9	1026.9	1026.9	1027.0	1027.2	1026.9
BAO+FS BOSS DR12	5.7	6.9	5.9	7.1	8.4	7.7	6.0
BAO BOSS low$-z$	1.8	2.7	2.1	2.2	2.8	1.7	2.2
eBOSS DR14 Lyman$-\alpha$	4.8	4.4	4.6	5.0	4.8	5.7	4.8
Planck high$-\ell$ TT,TE,EE	2356.7	2350.6	-	-	-	-	2365.4
Planck high$-\ell$ TT	-	-	768.5	773.8	774.2	-	-
Planck low$-\ell$ EE	396.7	395.7	395.7	395.8	395.8	-	395.7
Planck low$-\ell$ TT	25.5	25.2	24.3	21.3	21.0	-	25.1
Planck lensing	8.6	8.2	-	10.9	10.9	-	8.6
SPT high$-\ell$ TE,EE	-	-	147.8	-	-	-	-
SPT lensing	-	-	5.2	-	-	-	-
ACT DR4	-	-	-	-	-	275.2	-
ACT DR4 ($\ell_{\rm TT} > 1800$)	-	-	-	233.2	233.7	-	239.3
M_B Prior (SH_0ES 2021)	-	-	-	-	6.6	-	-
total	3826.7	3820.6	2381.0	2476.2	2485.2	1317.5	4074.0
total $\Delta\chi^2$	13.2	13.9	8.0	5.7	-9.6	-3.0	16.9
ΔAIC	17.2	17.9	12.0	9.7	-5.6	1.0	20.9

Table 7. Best-fit χ^2 per experiment (and total) from our CMB analyses in combination with BAO and SnIa in the pseudoscalar model. Per each run, we also report the corresponding $\Delta\chi^2 \equiv \chi^2_{\rm min,pseudo}$-$\chi^2_{\rm min,\Lambda CDM}$. In order to determine if the pseudoscalar model is favoured by the data in the analyses considered, we compute the AIC relative to that of ΛCDM (ΔAIC). Positive values prefer the ΛCDM model.

	Best-fit Pseudo vs CMB					
Parameter	*Planck*	*Planck* w. $A_{\rm lens}$	*Planck* TT+SPT	*Planck* TT+ACT	ACT	*Planck*+ACT
$100\,\omega_b$	2.263	2.307	2.265	2.213	2.156	2.223
$\omega_{\rm cdm}$	0.1219	0.1217	0.1226	0.1257	0.1265	0.1217
$100\,\theta_s$	1.04527	1.04527	1.04481	1.04686	1.04823	1.04653
$\ln 10^{10} A_s$	2.984	2.977	2.966	3.029	3.017	3.012
n_s	0.9435	0.9598	0.946	0.976	1.023	0.9536
$\tau_{\rm reio}$	0.0543	0.0519	0.0464	0.0559	0.06	0.0569
m_s [eV]	0.0	0.4	0.2	4.0	5.0	1.4
$\Delta N_{\rm eff}$	0.06	0.31	0.14	0.01	0.02	0.02
$A_{\rm L}^{\phi\phi}$		1.119				
$A_{\rm L}^{\rm TTTEEE}$		1.221				
H_0 [km/s/Mpc]	69.3	73.1	69.9	70.4	70.5	70.4
S_8	0.804	0.775	0.788	0.836	0.853	0.798
$\Delta\chi^2$	12.3	7.2	11.1	3.4	-5.3	17.4

Table 8. Best-fit values of the cosmological parameters from our CMB analyses in the pseudoscalar model. Per each run, we also report the corresponding $\Delta\chi^2 \equiv \chi^2_{\rm min,pseudo}$-$\chi^2_{\rm min,\Lambda CDM}$.

that we have performed to identify this multipole range. In Fig. 9 we examine the impact of different cuts in *Planck* polarization data. While restricting *Planck* TE-EE data to $\ell < 350$ and $\ell > 1000$, combined with *Planck* TT, makes the analysis in statistical agreement with ACT, this is no longer true when *Planck* TE-EE are restricted to $\ell < 500$ or $\ell > 900$.

C The CMB lensing anomaly in the non-interacting sterile neutrino model

The goal of this Appendix is to quantify the impact of marginalizing over the lensing information in *Planck* data in the presence of a non-interacting and free-streaming sterile neutrino species, and to compare the results with the ones discussed in Sec. 4.4 for the pseudoscalar model. To this end, in Fig. 10 we show the 1 and 2σ confidence regions for the non-interacting case. We note that the lensing anomaly is not relaxed even within such a scenario. We find

	Best-fit Pseudo vs CMB + BAO + SnIa						
Parameter	*Planck*	*Planck* w. $A_{\rm lens}$	*Planck* TT+SPT	*Planck* TT+ACT	$+H_0$	ACT	*Planck*+ACT
$100\,\omega_b$	2.257	2.272	2.284	2.210	2.201	2.157	2.224
$\omega_{\rm cdm}$	0.1222	0.1207	0.1213	0.1264	0.1271	0.1289	0.1225
$100\,\theta_s$	1.04525	1.04555	1.04481	1.04688	1.04678	1.04790	1.04584
$\ln 10^{10} A_s$	2.989	2.974	2.975	3.018	3.024	3.018	2.994
n_s	0.9416	0.9429	0.9448	0.974	0.977	1.016	0.9453
$\tau_{\rm reio}$	0.0563	0.0497	0.0517	0.0489	0.0510	0.057	0.0501
m_s [eV]	0.0	0.5	0.1	4.1	3.9	4.8	0.9
$\Delta N_{\rm eff}$	0.04	0.01	0.03	0.0	0.08	0.03	0.01
$A_{\rm L}^{\phi\phi}$		1.059					
$A_{\rm L}^{\rm TTTEEE}$		1.151					
H_0 [km/s/Mpc]	68.9	69.6	69.2	70.1	70.8	69.6	69.2
S_8	0.812	0.785	0.796	0.839	0.839	0.876	0.808
$\Delta\chi^2$	13.2	14	8	5.7	-9.6	-3.1	16.9

Table 9. Best-fit values of the cosmological parameters from our CMB analyses in combination with BAO and SnIa, in the pseudoscalar model. Per each run, we also report the corresponding $\Delta\chi^2 \equiv \chi^2_{\rm min,Pseudo}\text{-}\chi^2_{\rm min,\Lambda CDM}$.

that, as in the pseudoscalar case, in the non-interacting model the bounds on the sterile neutrino sector are not significantly modified by the introduction of the lensing parameters: a non-zero sterile neutrino mass is still allowed only in combination with $\Delta N_{\rm eff}$ values very close to zero. Moreover, as already discussed throughout the paper, the introduction of the lensing parameters non-trivially modifies the degeneracy between cosmological parameters, such that higher values of n_s, H_0 and $\Delta N_{\rm eff}$ are predicted when $A_{\rm L}^{\rm TTTEEE}$ and $A_{\rm L}^{\phi\phi}$ are let free to vary – albeit this trend is weaker than that observed in the pseudoscalar scenario (see Sec. 4.4). The impact on the CMB angular power spectra due to the preference for a higher value of n_s is shown in Fig. 11, where we compare the residuals of the pseudoscalar and the non-interacting best-fit power spectra with respect to the ΛCDM best-fit from *Planck* data alone, with and without marginalizing over the $A_{\rm L}^{\rm TTTEEE}$ and $A_{\rm L}^{\phi\phi}$ parameters. In fact, as expected, we see that both in the non-interacting and in the pseudoscalar model, the best-fit spectra corresponding to the analysis with free lensing parameters feature more power on high multipoles, particularly in the TT-spectrum.

D   Impact on the linear matter power spectrum

In Fig. 12 we show the best-fit residuals in the linear matter power spectrum with respect to the *Planck*-only ΛCDM best-fit, for the pseudoscalar model tested against *Planck*, *Planck* TT+SPT, *Planck* TT+ACT. In the upper panel we show the CMB-only cases, while in the lower panel we report the cases where BAO and SnIa are added to the analyses. As extensively discussed in Sec. 2, the pseudoscalar model does not induce a significant departure from the late-time matter distribution predicted by the ΛCDM model. The *Planck* TT+ACT prediction is the only case featuring an enhancement rather than a suppression of power, driven by the higher value of n_s, and responsible for the higher S_8 value obtained in this analysis. Finally, a comparison between the "*Planck*+$A_{\rm lens}$" residuals in the two panels visually shows why the inclusion of BAO and SnIa data sensibly alters the constraints on that case only, as discussed in Sec. 4.4.
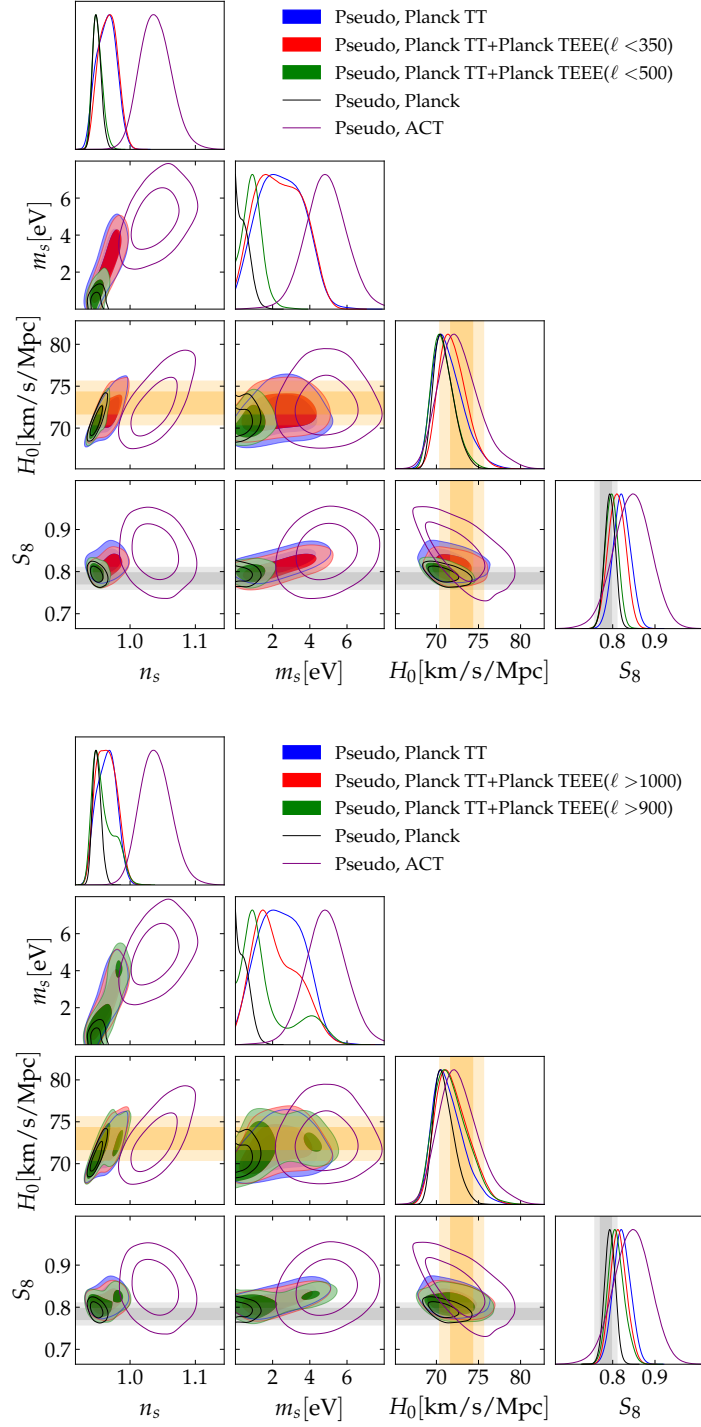
Figure 9. Posterior distributions of the cosmological parameters in the pseudoscalar (Pseudo) model for different subsets of *Planck* TE-EE data. The orange and gray bands represent the direct measurements (1 σ and 2 σ confidence regions) of H_0 and S_8, from cosmic distance ladder [9] and weak lensing observations [18], respectively.
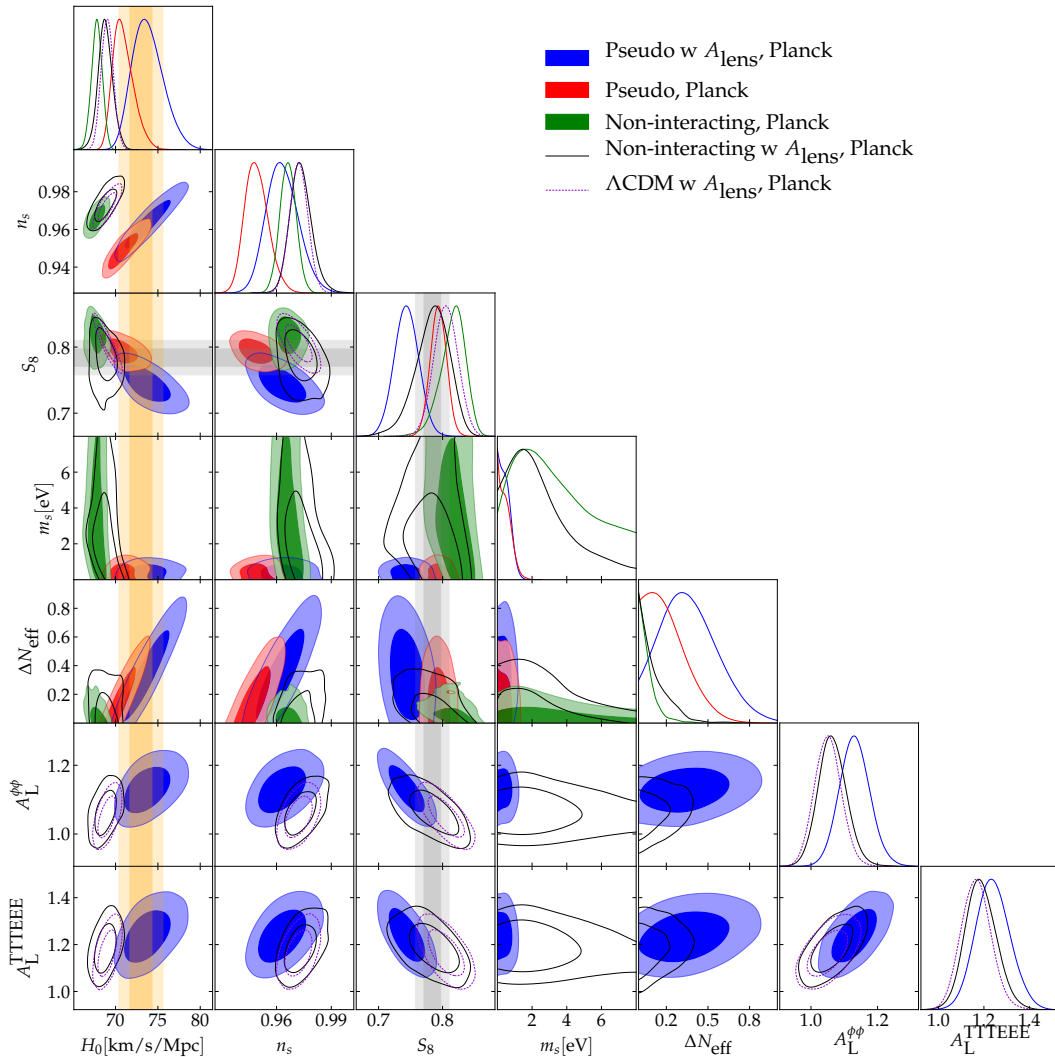
Figure 10. Posterior distributions of the cosmological parameters in the pseudoscalar (Pseudo) and free-streaming model tested with *Planck* data, with and without marginalizing over the gravitational lensing information. The orange and gray bands represent the direct measurements (1 σ and 2 σ confidence regions) of H_0 and S_8, from cosmic distance ladder [9] and weak lensing data [18], respectively.

References

[1] PLANCK collaboration, *Planck 2018 results. VI. Cosmological parameters*, *Astron.Astrophys.* **641** (2020) A6 [1807.06209].

[2] BOSS collaboration, *The clustering of galaxies in the completed SDSS-III Baryon Oscillation Spectroscopic Survey: cosmological analysis of the DR12 galaxy sample*, *Mon.Not.Roy.Astron.Soc.* **470** (2017) 2617 [1607.03155].

[3] EBOSS collaboration, *Completed SDSS-IV extended Baryon Oscillation Spectroscopic Survey: Cosmological implications from two decades of spectroscopic surveys at the Apache Point Observatory*, *Phys. Rev. D* **103** (2021) 083533 [2007.08991].

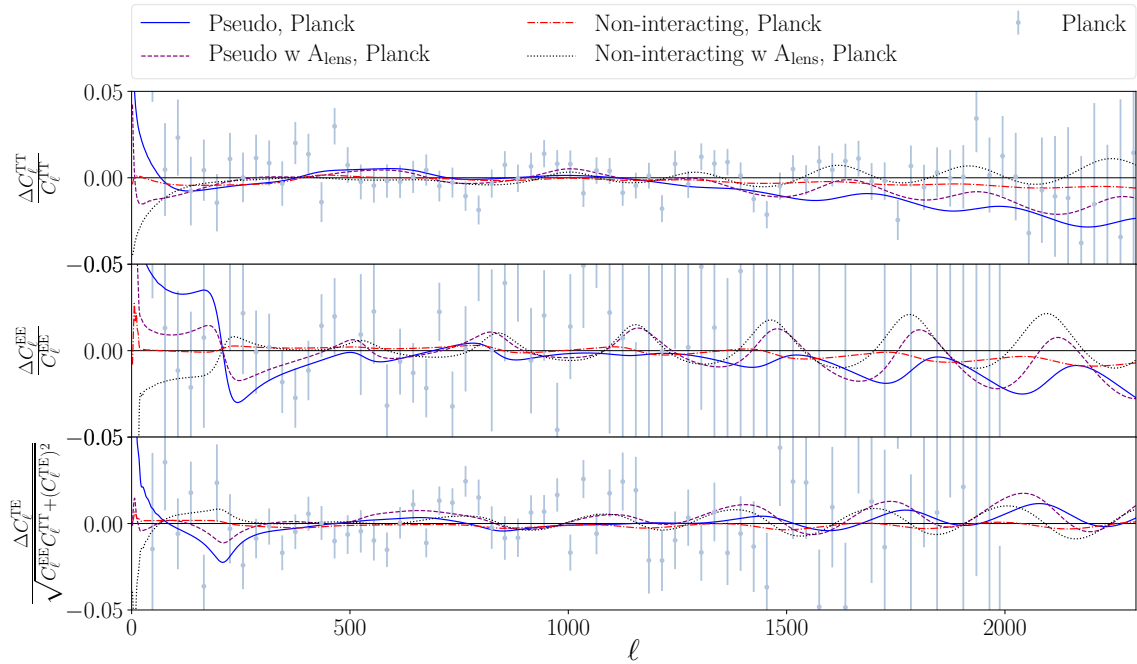[4] A.G. Riess, S. Casertano, W. Yuan, L.M. Macri and D. Scolnic, *Large Magellanic Cloud*

Figure 11. Residuals of the pseudoscalar and non-interacting models in the CMB TT, EE and TE power spectrum with respect to the *Planck*-only ΛCDM best-fit. We also show *Planck* data-points and error bars.
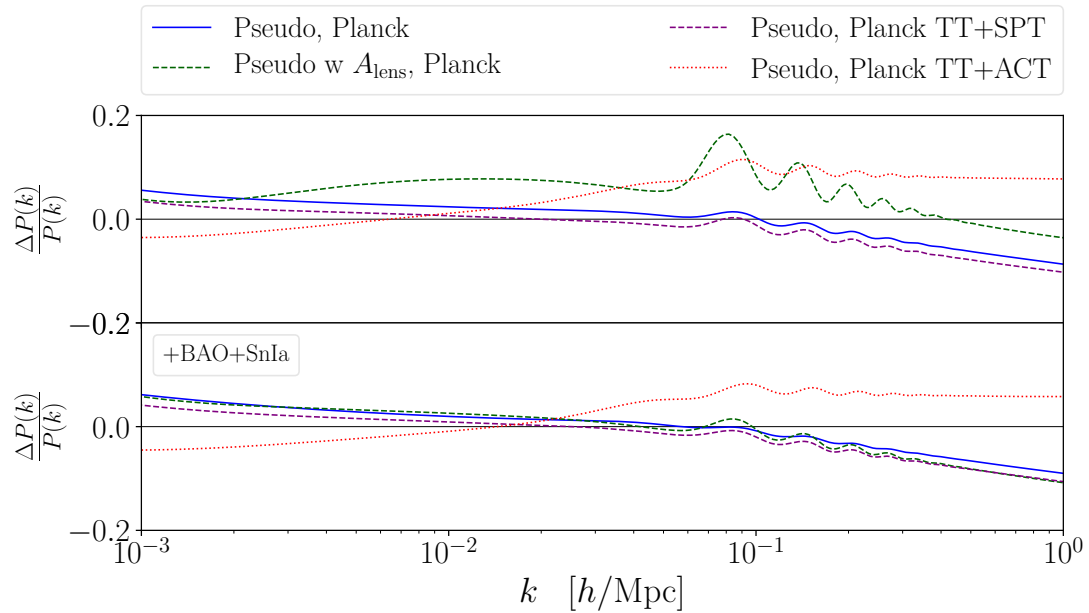

Figure 12. Linear matter power spectrum with residuals. For each model we show the relative difference between the pseudoscalar best-fit and the *Planck*-only ΛCDM best-fit.

Cepheid Standards Provide a 1% Foundation for the Determination of the Hubble Constant and Stronger Evidence for Physics beyond ΛCDM, *Astrophys.J.* **876** (2019) 85 [1903.07603].

[5] W.L. Freedman et al., *The Carnegie-Chicago Hubble Program. VIII. An Independent Determination of the Hubble Constant Based on the Tip of the Red Giant Branch*, 1907.05922.

[6] W. Yuan, A.G. Riess, L.M. Macri, S. Casertano and D. Scolnic, *Consistent Calibration of the Tip of the Red Giant Branch in the Large Magellanic Cloud on the Hubble Space Telescope Photometric System and a Re-determination of the Hubble Constant*, *Astrophys. J.* **886** (2019) 61 [1908.00993].

[7] W. Cerny, W.L. Freedman, B.F. Madore, F. Ashmead, T. Hoyt, E. Oakes et al., *Multi-Wavelength, Optical (VI) and Near-Infrared (JHK) Calibration of the Tip of the Red Giant Branch Method based on Milky Way Globular Clusters*, 2012.09701.

[8] J. Soltis, S. Casertano and A.G. Riess, *The Parallax of ω Centauri Measured from Gaia EDR3 and a Direct, Geometric Calibration of the Tip of the Red Giant Branch and the Hubble Constant*, *Astrophys. J. Lett.* **908** (2021) L5 [2012.09196].

[9] A.G. Riess et al., *Cosmic Distances Calibrated to 1EDR3 Parallaxes and Hubble Space Telescope Photometry of 75 Milky Way Cepheids Confirm Tension with LambdaCDM*, *Astrophys.J.* **908** (2021) L6 [2012.08534].

[10] M.G. Dainotti, B. De Simone, T. Schiavone, G. Montani, E. Rinaldi and G. Lambiase, *On the Hubble constant tension in the SNe Ia Pantheon sample*, *Astrophys. J.* **912** (2021) 150 [2103.02117].

[11] J.P. Blakeslee, J.B. Jensen, C.-P. Ma, P.A. Milne and J.E. Greene, *The Hubble Constant from Infrared Surface Brightness Fluctuation Distances*, *Astrophys. J.* **911** (2021) 65 [2101.02221].

[12] G.S. Anand, R.B. Tully, L. Rizzi, A.G. Riess and W. Yuan, *Comparing Tip of the Red Giant Branch Distance Scales: An Independent Reduction of the Carnegie-Chicago Hubble Program and the Value of the Hubble Constant*, 2108.00007.

[13] H. Hildebrandt et al., *KiDS+VIKING-450: Cosmic shear tomography with optical and infrared data*, *Astron.Astrophys.* **633** (2020) A69 [1812.06076].

[14] HSC collaboration, *Cosmology from cosmic shear power spectra with Subaru Hyper Suprime-Cam first-year data*, *Publ. Astron. Soc. Jap.* **71** (2019) 43 [1809.09148].

[15] S. Joudaki et al., *KiDS+VIKING-450 and DES-Y1 combined: Cosmology with cosmic shear*, *Astron.Astrophys.* **638** (2020) L1 [1906.09262].

[16] C. Heymans et al., *KiDS-1000 Cosmology: Multi-probe weak gravitational lensing and spectroscopic galaxy clustering constraints*, *Astron.Astrophys.* **646** (2021) A140 [2007.15632].

[17] DES collaboration, *Dark Energy Survey Year 3 Results: Cosmological Constraints from Galaxy Clustering and Weak Lensing*, 2105.13549.

[18] M. Gatti et al., *Dark Energy Survey Year 3 results: cosmology with moments of weak lensing mass maps*, 2110.10141.

[19] M. Rigault et al., *Confirmation of a Star Formation Bias in Type Ia Supernova Distances and its Effect on Measurement of the Hubble Constant*, *Astrophys. J.* **802** (2015) 20 [1412.6501].

[20] NEARBY SUPERNOVA FACTORY collaboration, *Strong Dependence of Type Ia Supernova Standardization on the Local Specific Star Formation Rate*, *Astron. Astrophys.* **644** (2020) A176 [1806.03849].

[21] L. Knox and M. Millea, *The Hubble Hunter's Guide*, *Phys.Rev. D* **101** (2020) 043533 [1908.03663].

[22] L. Verde, T. Treu and A.G. Riess, *Tensions between the Early and the Late Universe*, *Nature Astron.* **3** (2019) 891 [1907.10625].

[23] E. Di Valentino et al., *Snowmass2021 - Letter of interest cosmology intertwined II: The hubble constant tension*, *Astropart.Phys.* **131** (2021) 102605 [2008.11284].

[24] L. Perivolaropoulos and F. Skara, *Challenges for ΛCDM: An update*, 2105.05208.

[25] W.L. Freedman, *Measurements of the Hubble Constant: Tensions in Perspective*, *Astrophys.J.* **919** (2021) 16 [2106.15656].

[26] S. Camera, M. Martinelli and D. Bertacca, *Does quartessence ease cosmic tensions?*, *Phys. Dark Univ.* **23** (2019) 100247 [1704.06277].

[27] E. Di Valentino, A. Melchiorri, E.V. Linder and J. Silk, *Constraining Dark Energy Dynamics in Extended Parameter Space*, *Phys. Rev. D* **96** (2017) 023523 [1704.00762].

[28] G. Lambiase, S. Mohanty, A. Narang and P. Parashari, *Testing dark energy models in the light of σ_8 tension*, *Eur. Phys. J. C* **79** (2019) 141 [1804.07154].

[29] G.F. Abellan, R. Murgia, V. Poulin and J. Lavalle, *Hints for decaying dark matter from S_8 measurements*, 2008.09615.

[30] E. Di Valentino et al., *Cosmology intertwined III: $f\sigma_8$ and S_8*, *Astropart. Phys.* **131** (2021) 102604 [2008.11285].

[31] J.L. Bernal, L. Verde and A.G. Riess, *The trouble with H_0*, *JCAP* **10** (2016) 019 [1607.05617].

[32] K. Jedamzik, L. Pogosian and G.-B. Zhao, *Why reducing the cosmic sound horizon can not fully resolve the Hubble tension*, *Commun.in Phys.* **4** (2021) 123 [2010.04158].

[33] B.S. Haridasu, M. Viel and N. Vittorio, *Sources of H_0-tensions in dark energy scenarios*, *Phys.Rev. D* **103** (2021) 063539 [2012.10324].

[34] E. Di Valentino et al., *In the realm of the Hubble tension—a review of solutions*, *Class.Quant.Grav.* **38** (2021) 153001 [2103.01183].

[35] S. Vagnozzi, *Consistency tests of ΛCDM from the early integrated Sachs-Wolfe effect: Implications for early-time new physics and the Hubble tension*, *Phys.Rev.D* **104** (2021) 063524 [2105.10425].

[36] N. Schöneberg et al., *The H_0 Olympics: A fair ranking of proposed models*, 2107.10291.

[37] K.N. Abazajian et al., *Light Sterile Neutrinos: A White Paper*, 1204.5379.

[38] C. Giunti and T. Lasserre, *eV-scale Sterile Neutrinos*, *Ann.Rev.Nucl.Part.Sci.* **69** (2019) 163 [1901.08330].

[39] LSND collaboration, *Evidence for neutrino oscillations from the observation of $\bar{\nu}_e$ appearance in a $\bar{\nu}_\mu$ beam*, *Phys.Rev.D* **64** (2001) 112007 [hep-ex/0104049].

[40] MiniBooNE collaboration, *Significant Excess of ElectronLike Events in the MiniBooNE Short-Baseline Neutrino Experiment*, *Phys.Rev.Lett.* **121** (2018) 221801 [1805.12028].

[41] MiniBooNE collaboration, *Updated MiniBooNE neutrino oscillation results with increased data and new background studies*, *Phys. Rev. D* **103** (2021) 052002 [2006.16883].

[42] G. Mention, M. Fechner, T. Lasserre, T.A. Mueller, D. Lhuillier, M. Cribier et al., *The Reactor Antineutrino Anomaly*, *Phys.Rev.D* **83** (2011) 073006 [1101.2755].

[43] F. Kaether, W. Hampel, G. Heusser, J. Kiko and T. Kirsten, *Reanalysis of the GALLEX solar neutrino flux and source experiments*, *Phys.Lett.B* **685** (2010) 47 [1001.2731].

[44] SAGE collaboration, *Measurement of the solar neutrino capture rate with gallium metal. III: Results for the 2002–2007 data-taking period*, *Phys. Rev. C* **80** (2009) 015807 [0901.2200].

[45] C. Giunti and M. Laveder, *Short-Baseline Active-Sterile Neutrino Oscillations?*, *Mod. Phys. Lett. A* **22** (2007) 2499 [`hep-ph/0610352`].

[46] C. Giunti and M. Laveder, *Statistical Significance of the Gallium Anomaly*, *Phys.Rev.C* **83** (2011) 065504 [`1006.3244`].

[47] S. Gariazzo, C. Giunti, M. Laveder, Y.F. Li and E.M. Zavanin, *Light sterile neutrinos*, *J.Phys.G* **43** (2016) 033001 [`1507.08204`].

[48] S. Böser et al., *Status of Light Sterile Neutrino Searches*, *Prog.Part.Nucl.Phys.* **111** (2020) 103736 [`1906.01739`].

[49] J. Kopp, P.A.N. Machado, M. Maltoni and T. Schwetz, *Sterile Neutrino Oscillations: The Global Picture*, *JHEP* **05** (2013) 050 [`1303.3011`].

[50] M. Dentler et al., *Updated Global Analysis of Neutrino Oscillations in the Presence of eV-Scale Sterile Neutrinos*, *JHEP* **08** (2018) 010 [`1803.10661`].

[51] S. Gariazzo, C. Giunti, M. Laveder and Y.F. Li, *Updated Global 3+1 Analysis of Short-BaseLine Neutrino Oscillations*, *JHEP* **06** (2017) 135 [`1703.00860`].

[52] A. Diaz, C. Argüelles, G. Collin, J. Conrad and M. Shaevitz, *Where Are We With Light Sterile Neutrinos?*, *Phys.Rept.* **884** (2020) 1 [`1906.00045`].

[53] J.M. Berryman and P. Huber, *Sterile Neutrinos and the Global Reactor Antineutrino Dataset*, *JHEP* **01** (2021) 167 [`2005.01756`].

[54] C. Giunti, Y. Li, C. Ternes and Z. Xin, *Reactor antineutrino anomaly in light of recent flux model refinements*, `2110.06820`.

[55] J. Kostensalo, J. Suhonen, C. Giunti and P.C. Srivastava, *The gallium anomaly revisited*, *Phys.Lett.* **B795** (2019) 542 [`1906.10980`].

[56] V.V. Barinov et al., *Results from the Baksan Experiment on Sterile Transitions (BEST)*, `2109.11482`.

[57] V. Barinov and D. Gorbunov, *BEST Impact on Sterile Neutrino Hypothesis*, `2109.14654`.

[58] J.M. Berryman, P. Coloma, P. Huber, T. Schwetz and A. Zhou, *Statistical significance of the sterile-neutrino hypothesis in the context of reactor and gallium data*, `2111.12530`.

[59] MicroBooNE collaboration, *Search for an anomalous excess of charged-current quasi-elastic ν_e interactions with the MicroBooNE experiment using Deep-Learning-based reconstruction*, `2110.14080`.

[60] MicroBooNE collaboration, *Search for an anomalous excess of inclusive charged-current ν_e interactions in the MicroBooNE experiment using Wire-Cell reconstruction*, `2110.13978`.

[61] MicroBooNE collaboration, *Search for an Excess of Electron Neutrino Interactions in MicroBooNE Using Multiple Final State Topologies*, `2110.14054`.

[62] C.A. Argüelles, I. Esteban, M. Hostert, K.J. Kelly, J. Kopp, P.A.N. Machado et al., *MicroBooNE and the ν_e Interpretation of the MiniBooNE Low-Energy Excess*, `2111.10359`.

[63] P.B. Denton, *Sterile Neutrino Searches with MicroBooNE: Electron Neutrino Disappearance*, `2111.05793`.

[64] S. Gariazzo, P.F. de Salas and S. Pastor, *Thermalisation of sterile neutrinos in the early Universe in the 3+1 scheme with full mixing matrix*, *JCAP* **07** (2019) 014 [`1905.11290`].

[65] S. Hagstotz et al., *Bounds on light sterile neutrino mass and mixing from cosmology and laboratory searches*, `2003.02289`.

[66] S. Gariazzo, *Neutrino Properties and the Cosmological Tensions in the ΛCDM Model*, 2018 [`1812.00638`].

[67] S. Gariazzo, *Light Sterile Neutrinos In Cosmology*, in *17th Lomonosov Conference on Elementary Particle Physics Moscow, Russia, August 20-26, 2015*, 2016 [1601.01475].

[68] B. Dasgupta and J. Kopp, *Cosmologically Safe eV-Scale Sterile Neutrinos and Improved Dark Matter Structure*, *Phys.Rev.Lett.* **112** (2014) 031803 [1310.6337].

[69] S. Hannestad, R.S. Hansen and T. Tram, *How Self-Interactions can Reconcile Sterile Neutrinos with Cosmology*, *Phys.Rev.Lett.* **112** (2014) 031802 [1310.5926].

[70] M. Archidiacono, S. Hannestad, R.S. Hansen and T. Tram, *Cosmology with self-interacting sterile neutrinos and dark matter - A pseudoscalar model*, *Phys.Rev.D* **91** (2015) 065021 [1404.5915].

[71] C.D. Kreisch, F.-Y. Cyr-Racine and O. Doré, *Neutrino puzzle: Anomalies, interactions, and cosmological tensions*, *Phys.Rev.D* **101** (2020) 123505 [1902.00534].

[72] M. Archidiacono, S. Hannestad, R.S. Hansen and T. Tram, *Sterile neutrinos with pseudoscalar self-interactions and cosmology*, *Phys.Rev.D* **93** (2016) 045004 [1508.02504].

[73] M. Archidiacono, S. Gariazzo, C. Giunti, S. Hannestad, R. Hansen, M. Laveder et al., *Pseudoscalar–sterile neutrino interactions: reconciling the cosmos with neutrino oscillations*, *JCAP* **08** (2016) 067 [1606.07673].

[74] M. Archidiacono, S. Gariazzo, C. Giunti, S. Hannestad and T. Tram, *Sterile neutrino self-interactions: H_0 tension and short-baseline anomalies*, *JCAP* **12** (2020) 029 [2006.12885].

[75] E. Calabrese, A. Slosar, A. Melchiorri, G.F. Smoot and O. Zahn, *Cosmic Microwave Weak lensing data as a test for the dark universe*, *Phys. Rev. D* **77** (2008) 123531 [0803.2309].

[76] PLANCK collaboration, *Planck 2016 intermediate results. LI. Features in the cosmic microwave background temperature power spectrum and shifts in cosmological parameters*, *Astron.Astrophys.* **607** (2017) A95 [1608.02487].

[77] G. Efstathiou and S. Gratton, *A Detailed Description of the CamSpec Likelihood Pipeline and a Reanalysis of the Planck High Frequency Maps*, 1910.00483.

[78] P. Motloch and W. Hu, *Tensions between direct measurements of the lens power spectrum from Planck data*, *Phys.Rev. D* **97** (2018) 103536 [1803.11526].

[79] P. Motloch and W. Hu, *Lensing-like tensions in the Planck legacy release*, *Phys.Rev. D* **101** (2020) 083515 [1912.06601].

[80] SPT collaboration, *Measurements of the Temperature and E-Mode Polarization of the CMB from 500 Square Degrees of SPTpol Data*, *Astrophys.J.* **852** (2018) 97 [1707.09353].

[81] A. Chudaykin, D. Gorbunov and N. Nedelko, *Combined analysis of Planck and SPTPol data favors the early dark energy models*, *JCAP* **08** (2020) 013 [2004.13046].

[82] ACT collaboration, *The Atacama Cosmology Telescope: DR4 Maps and Cosmological Parameters*, *JCAP* **12** (2020) 047 [2007.07288].

[83] ACT collaboration, *The Atacama Cosmology Telescope: A Measurement of the Cosmic Microwave Background Power Spectra at 98 and 150 GHz*, *JCAP* **12** (2020) 045 [2007.07289].

[84] W. Handley and P. Lemos, *Quantifying the global parameter tensions between ACT, SPT and Planck*, *Phys.Rev. D* **103** (2021) 063529 [2007.08496].

[85] SPT-3G collaboration, *Measurements of the E-mode polarization and temperature-E-mode correlation of the CMB from SPT-3G 2018 data*, *Phys. Rev. D* **104** (2021) 022003 [2101.01684].

[86] A. Chudaykin, D. Gorbunov and N. Nedelko, *Exploring Early Dark Energy solution to the Hubble tension with Planck and SPTPol data*, *Phys.Rev. D* **103** (2021) 043529 [2011.04682].

[87] G.F. Abellán, R. Murgia and V. Poulin, *Linear cosmological constraints on 2-body decaying dark matter scenarios and robustness of the resolution to the S_8 tension*, 2102.12498.

[88] M.-X. Lin, W. Hu and M. Raveri, *Testing H_0 in Acoustic Dark Energy with Planck and ACT Polarization*, *Phys.Rev.D* **102** (2020) 123523 [2009.08974].

[89] S. Galli, L. Pogosian, K. Jedamzik and L. Balkenhol, *Consistency of Planck, ACT and SPT constraints on magnetically assisted recombination and forecasts for future experiments*, 2109.03816.

[90] J.C. Hill et al., *The Atacama Cosmology Telescope: Constraints on Pre-Recombination Early Dark Energy*, 2109.04451.

[91] V. Poulin, T.L. Smith and A. Bartlett, *Dark Energy at early times and ACT: a larger Hubble constant without late-time priors*, 2109.06229.

[92] G. Simard et al., *Constraints on Cosmological Parameters from the Angular Power Spectrum of a Combined 2500 deg^2 SPT-SZ and Planck Gravitational Lensing Map*, *Astrophys.J.* **860** (2018) 137 [1712.07541].

[93] SPT collaboration, *A Measurement of the Cosmic Microwave Background Lensing Potential and Power Spectrum from 500 deg^2 of SPTpol Temperature and Polarization Data*, *Astrophys.J.* **884** (2019) 70 [1905.05777].

[94] R. Murgia, G.F. Abellán and V. Poulin, *The early dark energy resolution to the Hubble tension in light of weak lensing surveys and lensing anomalies*, *Phys.Rev. D* **103** (2021) 063502 [2009.10733].

[95] N. Schöneberg, J. Lesgourgues and D.C. Hooper, *The BAO+BBN take on the Hubble tension*, *JCAP* **10** (2019) 029 [1907.11594].

[96] B. Audren, J. Lesgourgues, K. Benabed and S. Prunet, *Conservative Constraints on Early Cosmology: an illustration of the Monte Python cosmological parameter inference code*, *JCAP* **02** (2013) 001 [1210.7183].

[97] T. Brinckmann and J. Lesgourgues, *MontePython 3: boosted MCMC sampler and other features*, *Phys.Dark Univ.* **24** (2019) 100260 [1804.07261].

[98] D. Blas, J. Lesgourgues and T. Tram, *The Cosmic Linear Anisotropy Solving System (CLASS) II: Approximation schemes*, *JCAP* **07** (2011) 034 [1104.2933].

[99] PLANCK collaboration, *Planck 2018 results. VIII. Gravitational lensing*, *Astron.Astrophys.* **641** (2020) A8 [1807.06210].

[100] F. Bianchini et al., *Constraints on Cosmological Parameters from the 500 deg^2 SPTpol Lensing Power Spectrum*, *Astrophys.J.* **888** (2020) 119 [1910.07157].

[101] F. Beutler, C. Blake, M. Colless, D.H. Jones, L. Staveley-Smith, L. Campbell et al., *The 6dF Galaxy Survey: Baryon Acoustic Oscillations and the Local Hubble Constant*, *Mon.Not.Roy.Astron.Soc.* **416** (2011) 3017 [1106.3366].

[102] A.J. Ross et al., *The clustering of the SDSS DR7 main Galaxy sample – I. A 4 per cent distance measure at $z = 0.15$*, *Mon.Not.Roy.Astron.Soc.* **449** (2015) 835 [1409.3242].

[103] V.d.S. Agathe et al., *Baryon acoustic oscillations at $z = 2.34$ from the correlations of Lyα absorption in eBOSS DR14*, *Astron.Astrophys.* **629** (2019) A85 [1904.03400].

[104] M. Blomqvist et al., *Baryon acoustic oscillations from the cross-correlation of Lyα absorption and quasars in eBOSS DR14*, *Astron. Astrophys.* **629** (2019) A86 [1904.03430].

[105] D. Scolnic et al., *The Complete Light-curve Sample of Spectroscopically Confirmed SNe Ia from Pan-STARRS1 and Cosmological Constraints from the Combined Pantheon Sample*, *Astrophys.J.* **859** (2018) 101 [1710.00845].

[106] A. Gelman and D.B. Rubin, *Inference from Iterative Simulation Using Multiple Sequences*, *Statist. Sci.* **7** (1992) 457.

[107] A. Lewis, *GetDist: a Python package for analysing Monte Carlo samples*, `1910.13970`.

[108] F. James and M. Roos, *Minuit - a system for function minimization and analysis of the parameter errors and correlations*, *Computer Physics Communications* **10** (1975) 343.

[109] D. Camarena and V. Marra, *Local determination of the Hubble constant and the deceleration parameter*, *Phys. Rev. Res.* **2** (2020) 013028 [`1906.11814`].

[110] D. Camarena and V. Marra, *On the use of the local prior on the absolute magnitude of Type Ia supernovae in cosmological inference*, *Mon. Not. Roy. Astron. Soc.* **504** (2021) 5164 [`2101.08641`].

[111] A.G. Riess et al., *A Comprehensive Measurement of the Local Value of the Hubble Constant with 1 km/s/Mpc Uncertainty from the Hubble Space Telescope and the SH0ES Team*, `2112.04510`.

[112] H. Akaike, *A new look at the statistical model identification*, *IEEE Transactions on Automatic Control* **19** (1974) 716.

[113] M. Danilov, *New results from the DANSS experiment*, *PoS* **ICHEP2020** (2021) 121 [`2012.10255`].

[114] PROSPECT collaboration, *Improved short-baseline neutrino oscillation search and energy spectrum measurement with the PROSPECT experiment at HFIR*, *Phys. Rev. D* **103** (2021) 032001 [`2006.11210`].

[115] STEREO collaboration, *Improved sterile neutrino constraints from the STEREO experiment with 179 days of reactor-on data*, *Phys. Rev. D* **102** (2020) 052002 [`1912.06582`].

[116] K. Goldhagen, M. Maltoni, S. Reichard and T. Schwetz, *Testing sterile neutrino mixing with present and future solar neutrino data*, `2109.14898`.

[117] P.A. Machado, O. Palamara and D.W. Schmitz, *The Short-Baseline Neutrino Program at Fermilab*, *Ann. Rev. Nucl. Part. Sci.* **69** (2019) 363 [`1903.04608`].

[118] JSNS^2 collaboration, *Status and Prospects of the JSNS^2 Experiment*, *PoS* **ICHEP2018** (2019) 185 [`1811.03321`].

[119] L. Borodovsky et al., *Search for muon-neutrino oscillations muon-neutrino —> electron-neutrino (anti-muon-neutrino —> anti-electron-neutrino in a wide band neutrino beam*, *Phys. Rev. Lett.* **68** (1992) 274.

[120] KARMEN collaboration, *Upper limits for neutrino oscillations muon-anti-neutrino —> electron-anti-neutrino from muon decay at rest*, *Phys. Rev. D* **65** (2002) 112001 [`hep-ex/0203021`].

[121] NOMAD collaboration, *Search for nu(mu) —> nu(e) oscillations in the NOMAD experiment*, *Phys. Lett. B* **570** (2003) 19 [`hep-ex/0306037`].

[122] ICARUS collaboration, *Search for anomalies in the ν_e appearance from a ν_μ beam*, *Eur. Phys. J. C* **73** (2013) 2599 [`1307.4699`].

[123] OPERA collaboration, *Search for $\nu_\mu \to \nu_e$ oscillations with the OPERA experiment in the CNGS beam*, *JHEP* **07** (2013) 004 [`1303.3953`].

[124] T.L. Smith, M. Lucca, V. Poulin, G.F. Abellan, L. Balkenhol, K. Benabed et al., *Hints of Early Dark Energy in Planck, SPT, and ACT data: new physics or systematics?*, `2202.09379`.

[125] J.-Q. Jiang and Y.-S. Piao, *Towards early dark energy and n_s=1 with Planck, ACT and SPT*, `2202.13379`.

[126] CMB-S4 collaboration, *CMB-S4 Science Book, First Edition*, `1610.02743`.

[127] Simons Observatory collaboration, *The Simons Observatory: Science goals and forecasts*, *JCAP* **02** (2019) 056 [1808.07445].